METAL HYDRIDE THERMAL BATTERY DESIGN, LUMPED CAPACITANCE MODELING AND VALIDITY CRITERIA

by

Gareth D. Whatcott

A thesis submitted to the faculty of
The University of Utah
in partial fulfillment of the requirements for the degree of

Master of Science

Mechanical Engineering

The University of Utah

December 2013

The University of Utah Graduate School

STATEMENT OF THESIS APPROVAL

The thesis of **Gareth D Whatcott**

has been approved by the following supervisory committee members:

Kent Udell	, Chair	**July 23, 2013** Date Approved
Mathieu Francoeur	, Member	**July 23, 2013** Date Approved
Zhigang Zak Fang	, Member	**July 23, 2013** Date Approved

and by **Tim Ameel** , Chair/Dean of

the Department/College/School of **Mechanical Engineering**

and by David B. Kieda, Dean of The Graduate School.

ABSTRACT

In this thesis, the design and analysis of a dual bed metal hydride thermal battery is presented. First, a computer code that sizes the hydride bed cell to meet prescribed heat transfer goals is presented. A hypothetical bed shape is chosen and a matched pair of hydrides is optimized using the model. Various considerations are taken into account in selecting an appropriate configuration including ice buildup on the low temperature bed, pressure drop along the heat exchanger and cost. Second, a dynamic lumped capacitance kinetic model detailing the rate of hydrogen absorption and temperature change is presented. The model is validated against published data for a one bed constant pressure configuration, experimental data gathered for a second one bed constant pressure configuration and finally for a two bed thermal battery operating in heat pump mode. Third, it was found that each hydride should experience maximum kinetic rates at a temperature explicitly defined by the hydrides fundamental properties and the local hydrogen pressure. Finally, a finite difference model is developed to predict the radial temperature variation across the hydride cell cross section. It was found that the lumped capacitance model provides reasonable predictions of average cross-section temperatures as long as the kinetic rates, dimensions and thermal conductivity are such that a derived critical dimensionless ratio is less than 0.1.

CONTENTS

LIST OF FIGURES

LIST OF TABLES

NOTATION AND SYMBOLS

ΔH	Enthalpy of absorption (kJ/mol-H_2)
ΔS	Entropy of absorption (kJ/mol H_2-K)
δ	Ice thickness (m)
ϵ	Heat exchanger efficiency
ν	Kinematic viscosity (m^2/s)
ω	Specific humidity
ρ	Density (kg/m^3)
σ_y	Yield strength (Pa)
A_s	Surface area (m^2)
C_v	Flow coefficient
$C_{a,d}$	Pre-exponential coefficient (1/sec)
c_p	Specific heat (kJ/kg-K)
D_H	Hydraulic diameter (m)
E	Energy (J)
$E_{a,d}$	Activation energy (J/Mol H_2-K)
E_d	Energy density (kJ/kg)
f	Friction factor
h	Convective heat transfer coefficient (W/m^2-K)
h_f	Fin height (m)

h_{gs}	Enthalpy of formation (kJ/kg)
k	Thermal conductivity (W/m-k)
L	Length (m)
M	Molar mass (kg/kmol)
m	Mass (kg)
N	Number of cells
n	Number of fins
P	Pressure (Pa, bar)
Q	Power (W)
R	Universal gas constant
r	Radius (m)
T	Temperature (K)
t	Time (sec)
t_f	Fin thickness (m)
t_w	Wall thickness (m)
u	Fluid velocity (m/s)
V	Volume (m^3)
W	Wetted perimeter (m)
$WT\%$	Maximum hydrogen weight percent
X	Concentration ([H]/[M])
X_T	Pressure differential ratio factor

ACKNOWLEDGMENTS

I would like to acknowledge the assistance and guidance of my committee members, Prof. Mathieu Francoeur and Prof. Zak Fang. I want to especially thank my advisor, Prof. Kent Udell, who allowed me to work on his project and helped guide me through my research. I also want to thank him for his patience with me and willingness to spend additional time helping me complete this thesis. I want to thank my family and friends who provided encouragement and input to this project. I especially want to thank my wife, Barbara, who supported me and encouraged me throughout my time on campus. I know this was a long process for her and I want her to know how grateful I am for her continued support.

CHAPTER 1

DESIGN CONSIDERATIONS

The use of dual hydride beds for thermal energy storage and operating in heat pump mode has been of interest for many years [1]. A number of metal hydride heat pumps have been developed in a laboratory setting. Gruen was the first to create and analyze a prototype metal hydride heat pump [2]. Willers and Groll developed a two stage metal hydride heat transformer that was able to operate in a heat upgrading mode [3]. Sekhar, Pailwan and Muthukumar developed a single stage heat transformer for upgrading heat from around 400 K to 430 K [4]. Paya, Linder, Laurien and Corberan developed and analyzed a thermally driven metal hydride heat pump designed to remove waste heat from a high temperature source [5]. Yang, Wang, Zhang, Meng and Rudolph provided an overview of design considerations for metal hydride thermal batteries and heat pumps including thermal management, hydrogen transfer and mechanistic strength [6].

While laboratory scale systems have been developed, much of the mechanical engineering design analysis for building a full scale two-bed thermal battery has not been presented. This chapter will analyze a number of critical components when designing the integrated system. A theoretical metal hydride cell shape will be presented and optimized for a number of cells, number of fins, fin length and bed length.

This research has focused on developing a metal hydride thermal battery to be used in an electric automotive application. The thermal battery, operated as a heat pump, would replace an existing climate control system currently in the vehicle, allowing the electrochemical battery to be used for powering the vehicle as opposed to controlling the cabin temperature. The equations and methods developed are applicable to other applications with modification.

1.1 Metal Hydride Thermal Battery Operation

A metal hydride heat pump is a device constructed using two hydride beds, designed as a thermal battery capable of storing thermal energy to be used at a later time. Metal

hydrides are characterized as metals that bond with hydrogen to form a new compound in a reversible chemical reaction [7]. Hydrogenation of a metal hydride is an exothermic reaction according to equation 1.1.

$$2M + H_2 \leftrightarrow 2MH + \Delta H \tag{1.1}$$

The two operational modes for a metal hydride thermal battery are shown in Figure 1.1.

To charge the battery, heat is supplied to the high-temperature (HT) bed. This causes the hydrogen to become unbound. The hydrogen then travels to the low-temperature (LT) bed, where it is absorbed. This releases heat in the LT bed which requires some form of cooling to prevent the hydrogen absorption from coming to a stop.

During operation the valve connecting the two beds is opened, allowing hydrogen to flow from the high pressure bed (LT) to the low pressure bed (HT). As the hydrogen leaves the LT bed, heat is absorbed and the temperature decreases. As hydrogen is absorbed into the HT bed, heat is released and the temperature increase. Air is then passed over both beds, cooling the air moving over the LT bed and heating the air moving over the HT bed. This air is then available for either heating or cooling.

If no hydrogen leaks from the closed system, the dual-bed metal hydride thermal battery has an indefinite "shelf-life," allowing the system to be used for heating or cooling hours, days, months or years after being charged. This feature differentiates these thermal batteries from those that employ phase change or sensible heat storage.

1.2 Metal Hydride System Design

The primary design objective for a metal hydride heat pump is the determination of the proper sizing of the system to meet the performance requirements. The system is defined by the required energy(E_{out}) and power(Q_{out}) output along with the material properties of the hydrides and the container. The two hydrides also must be matched in the total amount of available hydrogen that can be released from one bed and absorbed into the other. Additionally, the total thermal mass of the system must be taken into account, as the hydrides must provide sufficient energy to meet the output demands along with raising or lowering the thermal mass to the operating temperature. With these considerations the optimal system will have the minimum amount of container mass possible while still meeting the energy and power output requirements.

The first parameter that needs to calculated is the mass of the metal hydride. To perform that analysis the enthalpy of absorption and desorption ($\Delta H_{a,d}$), for the HT and LT hydrides, respectively, needs to be known along with the maximum amount of hydrogen

that can be absorbed in weight percentage (WT%). For this analysis it will be assumed that the enthalpy of desorption for the LT bed is less than the enthalpy of absorption for the HT bed, making the LT bed the limiting hydride. If the reverse is true, then the subscripts in equations 1.3 and 1.4 should be switched from LT to HT and vice versa.

In order to calculate the mass of the metal hydride, an energy balance is performed.

$$E_{out} + (m_{LT}c_{p,LT} + m_c c_{p,c}) \left|T_i - T_{op}\right| = \frac{\Delta H_{LT} WT\%_{LT} m_{LT}}{M_{H_2}} \tag{1.2}$$

Rearranging equation 1.2 for m_{LT} yields:

$$m_{LT} = \frac{E_{out} + m_c c_{p,c} \left|T_i - T_{op}\right|}{\frac{\Delta H_{LT} WT\%_{LT}}{M_{H_2}} - c_{p,LT} \left|T_i - T_{op}\right|} \tag{1.3}$$

where T_i is the initial temperature of the bed and T_{op} is the operating temperature. To calculate the required mass of the HT hydride, a hydrogen mass balance is performed recognizing that the mass of hydrogen in both beds is the same.

$$m_{HT} = \frac{m_{LT} WT\%_{LT}}{WT\%_{HT}} \tag{1.4}$$

With the mass of both beds known the required internal volume of the container can be found using the metal hydride's packed powder density. This value can either be determined experimentally or approximated based on the raw density of the solid material. An appropriate density range for a packed powder bed is usually on the order of $.64\rho_o \leq \rho_{powder} \leq .75\rho_o$ [8, 9].

$$V_{LT,HT} = \frac{m_{LT,HT}}{\rho_{powder,LT,HT}} \tag{1.5}$$

In addition to the internal volume of the container, the total surface area of the container also needs to be known. This is found using the following energy balance on the surface and the minimum required power:

$$Q = \dot{m}_f c_f \epsilon \left|T_{f,in} - T_{op}\right| \tag{1.6}$$

where $T_{f,in}$ is the cooling fluid inlet temperature and ϵ is the heat exchanger efficiency defined as:

$$\epsilon = 1 - exp(-NTU) \tag{1.7}$$

and NTU is the number of transfer units defined as:

$$NTU = \frac{hA_s}{\dot{m}_f c_f} \tag{1.8}$$

Substitutin equations 1.7 and 1.8 into equation 1.6 and solving for A_s yields equation

1.9.

$$A_{s,LT} = \frac{-\dot{m}_f c_f}{h} ln\left(1 - \frac{Q}{\dot{m}_f c_f \left|T_{f,in} - T_{op}\right|}\right) \tag{1.9}$$

For the HT bed the only change in the required surface area calculation is the power required in the HT bed. Since it was assumed that $\Delta H_{a,HT} > \Delta H_{d,LT}$ then for the LT bed to remove enough hydrogen to meet the P_{min} requirement, the HT bed must absorb the same amount of hydrogen in the same amount of time. This yields the following relationship for the required power for the HT bed.

$$Q_{HT,min} = Q_{LT,min} \frac{\Delta H_{a,HT}}{\Delta H_{d,LT}} \tag{1.10}$$

The equations for the surface area for a given geometry will be a function of the number of cells, number of fins, fin dimensions and cell dimensions. It is also important to take into account the required strength of the container to hold the maximum operating pressure of the hydrogen. Thus the thickness of the container wall will be a function of the maximum internal hydrogen pressure.

With the required internal volume and outside surface area specified it is possible to optimize the number of cells, dimensions of the cell, number of fins per cell and fin dimensions for a given cell shape (cylindrical, rectangular, hexagonal, etc.). The optimization algorithm must be iterative because as the cell's relative size increases or decreases, the mass of the container will also change, which will affect the required amount of metal hydride according to equations 1.3 and 1.4. For these calculations, to ensure that the mass of the metal hydride is converging to a solution, a convergence criterion was specified as given in equation 1.11.

$$\frac{V_{SS,new} - V_{SS,old}}{V_{SS,new}} \leq 0.1 \tag{1.11}$$

The value of 0.1 was chosen as the criteria because for some configurations at more stringent convergence criterions, the system would enter an infinite loop and never converge. This value was found to provide sufficient accuracy while allowing for convergence in every configuration.

1.3 Energy Density Analysis

In order to compare different energy systems, an energy density analysis was be used. This allows for a more accurate comparison of two different energy systems. There are three levels at which energy density can be calculated for a metal hydride. These three methodologies are presented below.

1.3.1 Material Energy Density

The first level of energy density is at the material itself. This provides the maximum possible energy density for a given material and is defined in equation 1.12.

$$E_{d,mat} = \frac{WT\%\Delta H}{M_{H_2}} \tag{1.12}$$

This equation specifies the energy density of each material individually. It does not take into account the matching of two materials nor the mass required to contain the material. It is the most basic energy density definition and is most useful when used in the material selection phase of the design process.

1.3.2 Matched Pair Energy Density

The next level of energy density would be for a pair of metal hydrides. In order to build a system two hydrides must be matched in hydrogen storage capacity. This allows for all of the hydrogen to be desorbed from one bed and absorbed into another. Additionally, the energy density is specific to the mode of operation of the system, i.e., heating or cooling. For heating the energy density is:

$$E_{d,pair_{heat}} = \frac{E_{HT}}{m_{HT} + m_{LT}} \tag{1.13}$$

Rearranging the above equation and plugging in to solve for the masses and energy yields equation 1.14.

$$E_{d,pair_{heat}} = \frac{WT\%_{HT}\Delta H_{HT}}{M_{H_2}\left(1 + \frac{WT\%_{HT}}{WT\%_{LT}}\right)} \tag{1.14}$$

Similarly for the cooling mode the energy density can be shown to be:

$$E_{d,pair_{cool}} = \frac{WT\%_{LT}\Delta H_{LT}}{M_{H_2}\left(1 + \frac{WT\%_{LT}}{WT\%_{HT}}\right)} \tag{1.15}$$

1.3.3 System Energy Density

The final energy density is that for the entire system including container mass. Its specification is possible once a design has been selected and optimized as explained in Section 1.2. With the masses of the different metal hydrides, along with the container mass known, the system energy balance for heating can be defined as:

$$E_{d,sys_{heat}} = \frac{m_{HT}WT\%_{HT}\Delta H_{HT}}{M_{H_2}\left(m_{HT} + m_{LT} + m_c\right)} \tag{1.16}$$

The only thing that changes for the cooling mode is the energy portion in the numerator of the equation.

$$E_{d,sys_{cool}} = \frac{m_{LT} WT\%_{LT} \Delta H_{LT}}{M_{H_2} (m_{HT} + m_{LT} + m_c)} \tag{1.17}$$

The above energy density is useful in determining the efficiency of the system design. Since the matched pair energy density is the maximum possible energy density for the given metal hydride pair, a system efficiency can be defined as:

$$\eta_{sys} = \frac{E_{d,sys}}{E_{d,pair}} \tag{1.18}$$

The system efficiency is a useful parameter to assess energy dilution from the chemically inert container mass.

1.3.4 Conventional System Energy Density

To justify the installation of a metal hydride heat pump into an electric vehicle, the system must have a higher energy density than just installing additional batteries to power the conventional heat pump climate control system. To compare the two systems the following must be known about the conventional system installed: mass of the components, energy requirement, battery mass and battery energy. The basic form of energy density for a conventional system is the energy required to operate the system divided by the mass of the system plus the mass of the battery required to power the system. This is shown in equation 1.19.

$$E_d = \frac{E_{conv.}}{m_{conv.} + m_{batt.}} \tag{1.19}$$

This form of energy density allows for an accurate comparison between a conventional system and a metal hydride system. By taking into account the mass of the batteries required to power the conventional system, the same amount of energy is available to drive the vehicle.

It should be noted that the energy required to operate the fans in the metal hydride system have been neglected. When fans are chosen the energy of the fans should be included in the numerator of equation 1.16 and the mass of the fans, along with the mass of the batteries required to power the fans, should be included in the denominator.

1.4 Cold Bed Ice Buildup

Another design consideration for a metal hydride heat pump is the potential of ice build-up on the cold hydride operating in heating mode on cool, high humidity days. The build up of ice has the potential to block airflow passages adjacent to the hydride if the

spacing between cells is insufficiently large. This blockage would significantly decrease the heat transfer to the low temperature hydride system, lowering the hydrogen release rate, thus affecting the high temperature bed performance. To assess this failure mode, the amount of ice build up that would occur in the worst-case scenario is calculated.

1.4.1 Energy Balance

To calculate the thickness of the ice, the following first order assumptions are made. Since the maximum ice thickness is desired, the inlet air that is passed over the cells is assumed to have a 100% relative humidity. It is also assumed that the ice is evenly distributed over the hydride container surface. The temperature of the cold hydride remains below the inlet air temperature and below the freezing point of water.

For a given air mass flow rate and heat transfer rate from the cylinder, there is a fixed air temperature change across the heat exchanger. The relationship between these variables is defined from an energy balance. Under steady state conditions, the metal hydride dehydrogenation rate is nearly constant. Since the enthalpy of hydrogenation is also constant, the heat transfer to the cold hydride is fixed at a value denoted by $\dot{Q}_L$. That is equal to the energy lost from the air stream through convective heat transfer and due to ice deposition:

$$c_{p,f}(T_{f,in} - T_{f,out})\dot{m}_f + (\omega_{f,in} - \omega_{f,out})h_{gs}\dot{m}_f = \dot{Q}_L \tag{1.20}$$

where T_{in} is the inlet air temperature, $T_{f,out}$ is assumed to be the worst case scenario, which would be the hydride surface temperature, and h_{gs} is the enthalpy of deposition and is defined by the linear interpolation in equation 1.21 from published data [10].

$$h_{gs} = 2453.9 + 47.4 - \frac{T_{f,in}}{20} \tag{1.21}$$

The total mass of ice, m_{ice}, that will form on the heat exchanger in a given time, t, is described by equation 1.22.

$$m_{ice} = (\omega_{f,in} - \omega_{f,out})\dot{m}_f t \tag{1.22}$$

The thickness of ice, δ, formed is found from equating the ice mass to the volume of ice multiplied by the density:

$$m_{ice} = \rho_{ice} V_{ice} = \rho_{ice}(WL\delta) \tag{1.23}$$

where W is the wetted perimeter and L is the length of the hydride bed.

1.4.2 Equations of State for Air

To calculate the average ice thickness, the difference in specific humidity needs to be specified. The specific humidity of air with a relative humidity of 100% is defined from the total gas pressure and the water vapor pressure as follows.

$$\omega = \frac{0.622 P_{sat}}{P - P_{sat}} \tag{1.24}$$

The water saturation pressure, P_{sat}, is a function of temperature. The Clausius-Clapeyon equation was integrated to obtain a relation between the saturation pressure and the temperature, T:

$$P_{sat} = P_{\circ} exp\left[\frac{h_{fg}}{R_f}\left(\frac{1}{T_{\circ}} - \frac{1}{T}\right)\right] \tag{1.25}$$

where P_o and T_o are a known saturation pressure and temperature and h_{fg} is the enthalpy of vaporization. For this equation pressure is in Pascals. Thus for a constant total pressure, ω can be specified explicitly by the temperature.

1.5 Implementation and Results

To demonstrate the usefulness of the above calculations a pair of metal hydrides has been chosen along with a basic cell geometry. The material chosen for the HT bed is $MgH_2{-}0.1TiH_2$ and the material chosen for the LT bed is $LaNi_5$. These materials were chosen based on the materials properties and experimental data that is available, and they do not necessarily represent an ideal or optimum pair of hydrides for an efficient metal hydride heat pump. Table 1.1 shows the material properties of the materials chosen. The material properties for both materials were found in the literature [11, 12].

The cell shape was chosen to be cylindrical and the fins were chosen to run longitudinally along the cell. The properties of the container and some of the assumptions about the air flow and fin geometry are summarized in Table 1.2.

1.5.1 Cell Specific Equations

In order to accurately model the system, some of the equations outlined in Section 1.2 and Section 1.4 need to modified for the specific geometry being used.

First, the inside radius of the cylinder needs to be defined. This is done by using equation 1.5 and specifying the volume of a cylinder. This yields:

$$r_{in} = \sqrt{\frac{m}{\rho_{powder} L N \pi}} \tag{1.26}$$

where N is the number of cells in the system and L is the length of each cell.

Next the thickness of the cell wall is determined by calculating the stress in the cell. Since the cell is cylindrical, the hoop stress is used to determine the wall thickness. The cell is assumed to be thin-walled. This assumption will be verified by using the thin-walled pressure vessel criteria of $10t_w \leq d_{in}$. Equation 1.27 shows the relation of the pressure and yield strength to the wall thickness.

$$t_w = \frac{P_{max} r_i SF}{\sigma_y} \tag{1.27}$$

With the thickness and the inside radius known the outside radius is just the summation of the two values

With the outside radius known, the number of fins needed can be determined for a given fin height and thickness. This is done by using the required surface area calculated in equation 1.9. With the required surface area known, along with the geometry of the fins and cells, the surface area can be found using equation 1.28.

$$A_s = LN(2\pi r_o + 2nh_f - nt_f) \tag{1.28}$$

Solving for n yields:

$$n = \frac{A_s - 2LN\pi r_o}{LN(2h_f - t_f)} \tag{1.29}$$

The value of n specified by equation 1.29 should be rounded up to the nearest whole number to ensure that the surface area is sufficient to meet the power requirements. The method used to determine the fin height and the fin thickness will depend on the geometric constraints of the application.

The thickness of the ice buildup on the cell also needs to be calculated and used as a qualifying value for sufficient separation between adjacent fins. The mass of the ice is calculated in equation 1.22 and can be equated to equation 1.23, where the volume of the ice is calculated. For a finned cylinder the volume is found to be:

$$V_{ice} = NL(\delta^2\pi + r_o\delta\pi - \delta t_f n + 2nh_f\delta - 2n\delta^2) \tag{1.30}$$

Substituing equation 1.30 into equation 1.23 and solving for δ using the quadratic formula yields:

$$\delta = \frac{-NL\rho_{ice}(r_o\pi + 2nh_f - t_f n) + \sqrt{NL\rho_{ice}(r_o\pi + 2nh_f - t_f n)^2 + 4m_{ice}NL\rho_{ice}(\pi - 2n)}}{2NL\rho_{ice}(\pi + 2n)} \tag{1.31}$$

The pressure drop through the heat exchanger is also of interest. It is quantified by first calculating the hydraulic diameter of the heat exchanger according to the equation

$D_H = 4A_f/W$, where A_f is the area the fluid passes through and W is the wetted perimeter of the heat exchanger. These are defined in equations 1.32 and 1.33.

$$A_f = A_{Tot} - A_{Occupied} = N\sqrt{12}\left(r_o + \frac{h_f}{2}\right)^2 - N(\pi r_o^2 + nh_f t_f) \tag{1.32}$$

$$W = N(2\pi r_o + 2nh_f - nt_f) \tag{1.33}$$

The total area, A_{Tot} is found by assuming the cells are in a tightly packed configuration. This means that the fins are arranged such that there is no interference between fins and that a perfectly vertical or horizontal fin is allowed to touch the adjacent cell. In this type of configuration the packing efficiency of cylinders is $\eta_{pack} = \pi/\sqrt{12}$ [13]. Using this value the total area can be approximated as the area of the cylinder with a diameter of r_o plus half the fin height divided by η_{pack}. Figure 1.2 shows a hypothetical configuration with the dotted lines representing the diameter of the cylinder used to calculate the total area occupied by the system. It is important to note that the fins of the outside cells are not touching any adjacent cell. This results in the actual total occupied area being slightly higher than what is being calculated. Because of this, the calculated pressure drop will be greater than the actual pressure drop and the calculated volume will be less than the actual volume.

With the hydraulic diameter calculated, the Reynolds number can be found and used to calculate the pressure drop along the heat exchanger using Bernoulli's principle and the Colebrook equation. For these calculations air is modeled as an incompressible fluid. This assumption is valid for mach numbers less than 0.3 [14].

$$Re = \frac{uD_H}{\nu} \tag{1.34}$$

$$\Delta P = f_d \frac{L}{D_H} \frac{u^2 \rho_{air}}{2} \tag{1.35}$$

$$\frac{1}{\sqrt{f_d}} = -2\log\left(\frac{\epsilon}{3.7D_H} + \frac{2.51}{Re\sqrt{f}}\right) \tag{1.36}$$

1.5.2 Methodology

With the necessary equations developed for the specific geometry, the method of analysis applied will be discussed. Most of the above equations require an iterative approach to converge to a solution. For example, the mass of the container is unknown when the calculations begin. Mass determines, in addition to the energy requirements, the amount of metal hydride required, which then affects the size of the container and the required

number of fins, which will in turn change the mass of the container. A flow diagram for the algorithm used is shown in Figure 1.3.

The algorithm used is highly dependent on the objectives of the design. For this example, the primary objective was to minimize the volume with a secondary objective of minimizing the mass. Because of this the fin height was initialized to a minimum value and then iterated upwards until a feasible configuration was found, yielding the smallest volume configuration for the number of cells chosen.

1.5.3 Results

To evaluate the performance of configurations similar to that shown in Figure 1.2, a computer code was developed in Matlab to perform the necessary iterations.

Figures 1.4 and 1.5 show the mass of the hydride and container for both the HT and LT beds, respectively. The mass of the system decreases as the number of cells increases. This seems intuitive due to the fact that the volume of the container decreases proportional to the square of the outside radius while the surface area decreases linearly with the radius. In other words, to meet surface area requirements it is better gravimetrically to have lots of small cells. The outside radius of each individual cell is shown for both the HT and LT beds in Figures 1.6 and 1.7.

The discontinuous nature of the calculations presented in Figures 1.4 and 1.5 is due to the fact that the calculation of the surface area requirement is performed with discrete numbers of fins. When the surface area is calculated, a minimum integer number of fins are added to satisfy the surface area, thus the surface area of the cell is always greater than the exact surface area required. Often the iterated surface area required is only slightly more than what can be provided with one less fin. As the number of cells increases the radius of the cell decreases. This amounts to a net gain in total surface area: more cells with slightly less area. As this occurs, a lesser number of fins is needed. For systems with a small number of large cells with many fins, the drop in fins is fairly consistent, reducing the variation in mass, resulting in a smoother plot. For systems with a large number of smaller cells, the reduction in fin numbers is much slower, as shown in Figures 1.8 and 1.9. What is occurring at the jagged points is that the number of fins required on each cell is decreasing by one. When this happens there is a drop in the total mass. On the next iteration the number of cells is increased by one, the total surface area increases slightly but not enough to reduce the number of fins, resulting in a net increase in mass from the previous iteration. This is why after the sudden drop in mass, the system mass begins to increase gradually. It also

explains why the feature is more significant for the cells with the longer length than for the shorter cells since more mass is being removed when the number of fins is reduced.

Figures 1.10 and 1.11 show the total volume of the bed, including the container, fins and air spaces, for the HT and LT beds, respectively. These figures show that as the number of cells is increased in a bed, the total volume of that bed increases. This is opposite the result of the mass and leads to a difficult engineering problem. If the volume is optimized, the mass will be near its maximum and if the mass is optimized the volume will be near a maximum. This paradox becomes a problem of engineering judgement, since there is not a single configuration that is both gravimetrically and volumetrically ideal. Other considerations must be taken into account that are described in the following figures.

An interesting feature of the volume plots is the local minimum that occurs at very low N values. This feature is due to fin height. As mentioned earlier, minimizing the volume was a primary objective of this algorithm. Thus a minimum fin height was selected and the number of fins needed for a given number of cells was calculated. If there was not enough room on the cell to place all of those fins, either due to ice buildup interference between fins or simply too many fins on too small a cylinder, then the fin height was incrementally upped and the system was resized. This was repeated until a configuration was found that had enough space to house the number of fins required.

At low N values, the fin height is decreasing with an increasing number of cells while the number of fins is either increasing or remaining constant. This can be seen in Figures 1.8 and 1.9. Therefore, even though the number of cells is increasing, the total volume is decreasing since the fin height is decreasing as well. This happens until the minimum fin height is reached. At that value, a minimum volume is achieved and then the volume begins increasing as the the number of cells increases.

One of the first considerations that should be addressed is the manufacturability of the bed. This will help determine which of the configurations would be best to select. Figures 1.8 and 1.9 show the number of fins required on each cell for the HT and LT beds. These plots show that for a small number of cells there is a very large number of fins, making manufacturing much more difficult to accomplish. It also shows that there is a point of diminishing returns for increasing the number of cells to reduce the number of fins. On both the HT and LT beds, it is clear that the manufacturing benefit for increasing the number of cells is drastically reduced around the 15 to 20 cell range, depending on what length of cell is used.

As mentioned earlier, the number of fins has some interesting effects on both the volume

and the mass of both the HT and LT beds. It is difficult to discern from the figures, but the number of fins is a step function and not a smooth plot. Under close examination it can be seen that the number of fins is decreasing incrementally at high N values and that those steps correspond to sharp decreases in mass.

Another consideration that will aid in the selection of the cell configuration is the pressure drop of the air over the length of the bed, which is shown in Figures 1.12 and 1.13. This pressure drop will determine the size of the fan required for a given flow rate. The allowable size of the fan will be determined by the application in which the heat pump will be used. For the case of an electric vehicle the fan should be relatively small to limit noise and power from the battery. At the flow rate chosen (.113 m^3/sec), an ideal 100 W fan would have a pressure drop of around 1000 Pa [15] and falls in the range of diminishing returns for increasing the number of cells. Again, this is around 10 to 20 cells where the benefits of increasing the number of cells produces a diminishing reduction in the pressure drop.

To assist in selecting an ideal bed, a cost function was developed. The form of the function is given in equation 1.37:

$$cost = a(N_{LT} + N_{HT}) + b(n_{LT} + n_{HT}) + c(L_{LT} + L_{HT}) \tag{1.37}$$

where a, b and c are cost ratios relating the total cost of the cell component to the cost of the system. For convenience, the three ratios should add up to 1 signifying that the combined costs of the three components represent the total cost of manufacturing the array.

Using the above equation and estimated coefficients of $a = 0.5$, $b = 0.4$ and $c = 0.1$, Figure 1.14 is generated.

Using the cost function and the cost coefficients described above, the pair of HT and LT beds with the minimum cost was found. The detailed results for this selection are given in Table 1.3 along with the energy density for the total system. Additionally, a sample arrangement for the minimum cost HT and LT beds is shown in Figure 1.15.

From these data, the assumption used earlier that the vessel is thin walled can be verified. For both the LT and HT bed it is clear that $10t_w$ is less than d.

It is apparent that even though this configuration does represent the minimum cost, it does not necessarily meet all the requirements for the bed. For example, the pressure drop along the length of the HT bed is above 1000 Pa, meaning a fan larger than 100 W will be needed. This may be an unacceptable result, forcing the designer to select a different configuration. The cost function helps provide guidance but additional considerations

should also be analyzed.

For comparison, based on equation 1.19 and conversations with a GM Lab Group Manager in the Vehicle Development and Research Lab (B. Khalighi, Personal Conversation, May 6, 2013), the energy density for a conventional HVAC system in a Chevy Volt is 280 kJ/kg. This comparison demonstrates that the metal hydride heat pump selected in this analysis is not superior to currently installed technology. Improvement in energy density can be made by selecting a configuration with less mass, but at the expense of pressure drop, volume, manufacturability and cost.

The energy density of the metal hydride heat pump can be drastically improved by using a cold hydride with a higher storage capacity, a lower density or a higher enthalpy of desorption. $LaNi_5$ has a relatively low enthalpy of desorption compared with the magnesium hydride, a high density and a low storage capacity. Using a LT hydride with improvement in any of these three properties would improve the energy density of the system, potentially making it comparable, if not an improvement, to current technologies in terms of energy density.

1.6 Conclusion

An algorithm for the design and sizing of a dual bed metal hydride thermal battery was developed and used to define specific configurations capable of meeting heat transfer and energy storage metrics. Considerations were made for ice buildup on the LT bed, pressure loss along the length of the heat exchanger and cost. An example matched hydride dual bed system was analyzed and the energy density was found to to be less than currently installed HVAC technology. Higher energy densities can be achieved for systems with improved LT bed metal hydrides or by selecting a configuration with lower mass at the expense of increased volume.

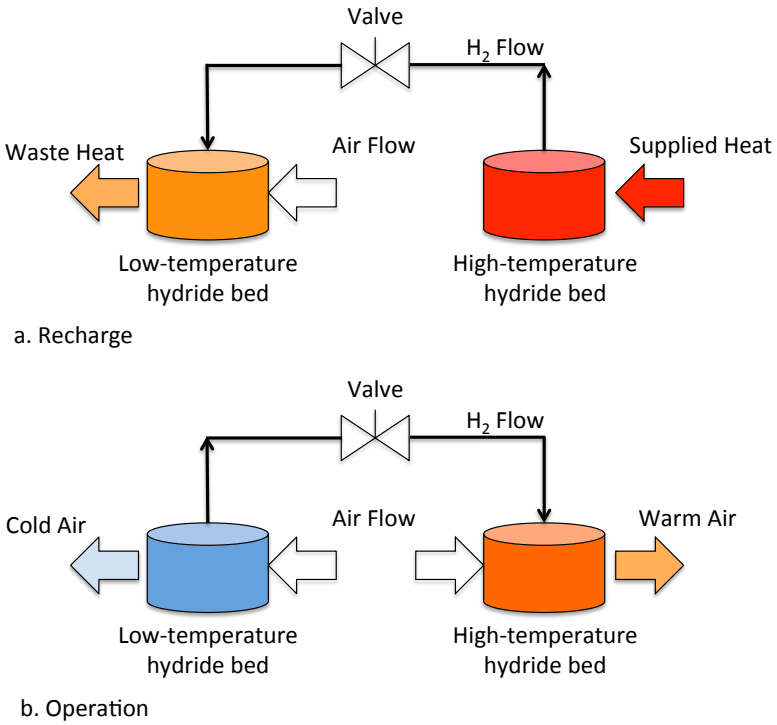

Figure 1.1. Metal hydride thermal battery operation. a. Charging cycle for a metal hydride thermal battery. Heat is supplied to the high-temperature hydride, liberating the hydrogen from the high-temperature bed and absorbed in the low-temperature bed. Air is supplied to the low-temperature bed to maintain the absorption rates. b. Heat pump mode for metal hydride thermal battery. Hydrogen is allowed to desorb from the low-temperature bed, causing the bed temperature to drop, and is absorbed in the high temperature bed, causing the bed temperature to rise. Air is passed over both beds to be used for either heating or cooling.

Table 1.1. Material properties of selected metal hydrides

	ρ (kg/m^3)	Packing Density (%)	c_p (kJ/kg-K)	ΔH (kJ/mol H_2)	WT%
MgH_2−0.1TiH_2	1660	40	1.02	68.2	6
$LaNi_5$	8300	69	.419	30.8	1.28

Table 1.2. System properties and constants

Constant (Symbol)	Value	Units
Yield Strength SS (σ_y)	170	MPa
Specific Heat SS ($c_{p,SS}$)	0.5	kJ/kg-K
Density SS(ρ_{SS})	8000	kg/m^3
Roughness SS (ϵ)	1.5×10^{-5}	m
Pressure (P_{max})	20	Bars
Safety Factor (SF)	5	
Minimum Fin Height ($h_{f,min}$)	0.48	cm
Fin Thickness(t_f)	0.5	mm
Cooling Outside Air Temp ($T_{f,i,cooling}$)	35	C
Heating Outside Air Temp ($T_{f,i,heating}$)	15	C
HT Bed Temperature	150	C
LT Bed Temperature	-10	C
Convective Heat Transfer Coefficient (h)	20	W/m^2-K
Air Flow Rate($\dot{V}_{air}$)	.113	m^3/sec

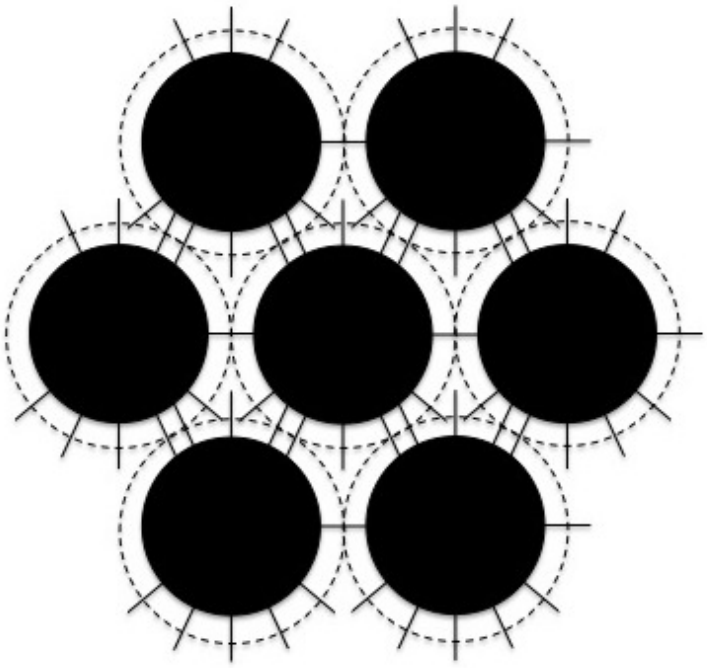

Figure 1.2. Sample array consisting of 7 cells with 8 fins each. The dotted lines represent the diameter used to calculate the total area occupied by the system.

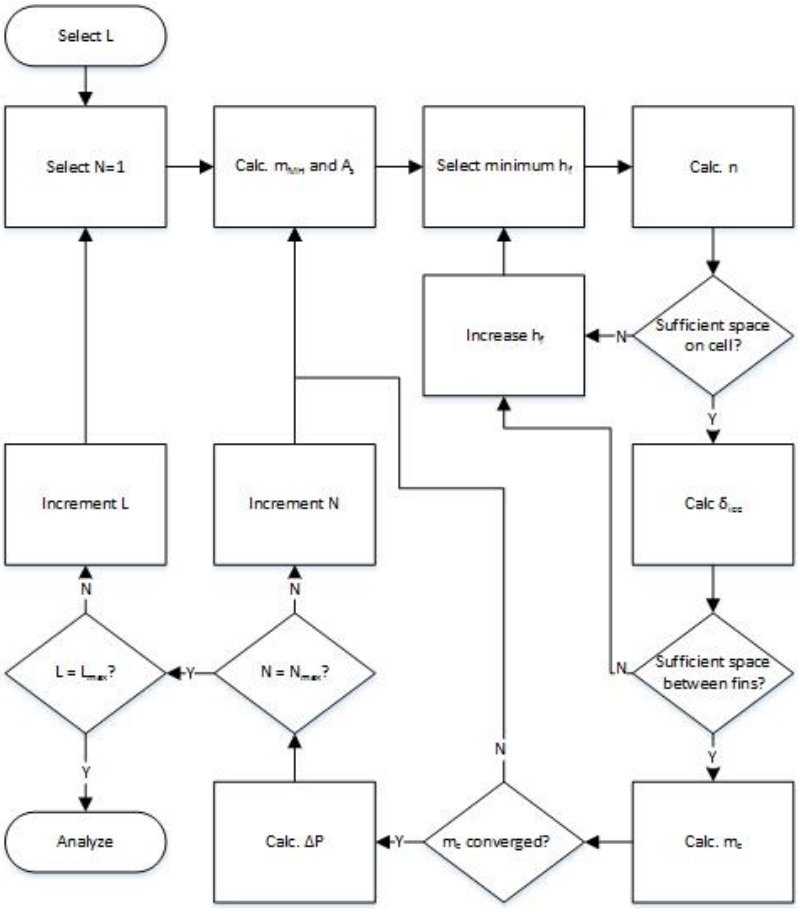

Figure 1.3. Optimization algorithm flow diagram. Optimization algorithm used for cylindrical cell shape. The length, number of cells and fin height are the variables while the mass of the metal hydrides and the number of fins are the dependent variables. The pressure drop, ice buildup and total volume are calculated

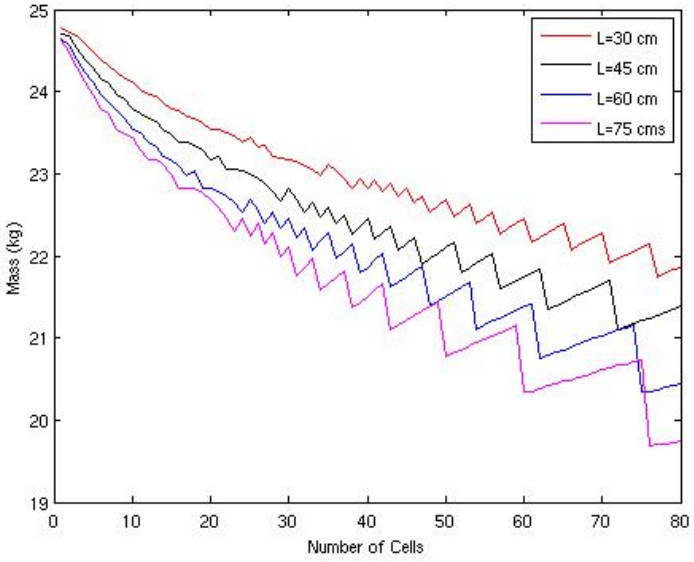

Figure 1.4. Cylindrical HT bed mass. Total mass of HT bed for various cell lengths and for differing numbers of cells.

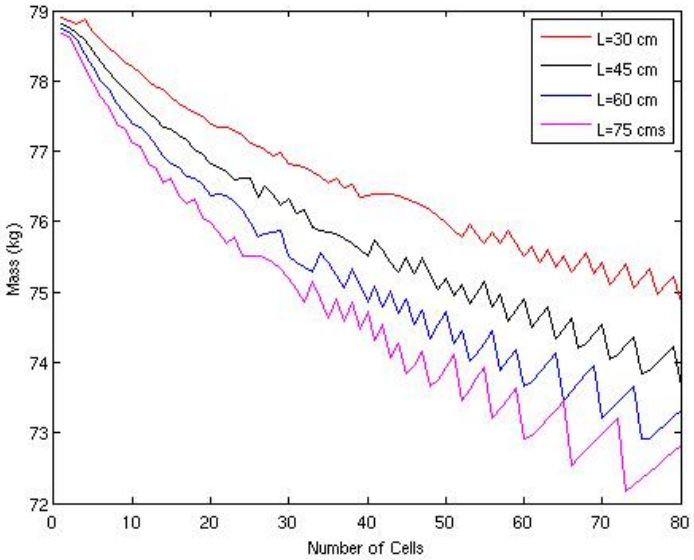

Figure 1.5. Cylindrical LT bed mass. Total mass of LT bed for various cell lengths and for differing numbers of cells.

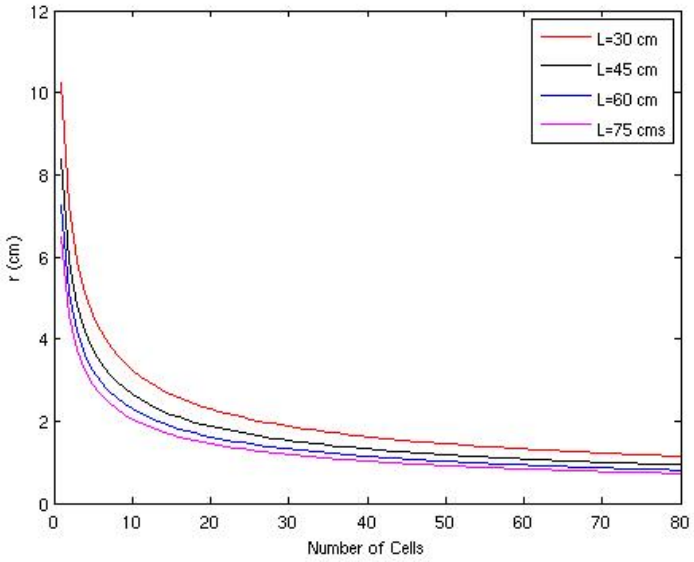

Figure 1.6. Cylindrical HT bed outside radius. Outside radius of a single HT bed cell for various cell lengths and for differing numbers of cells.

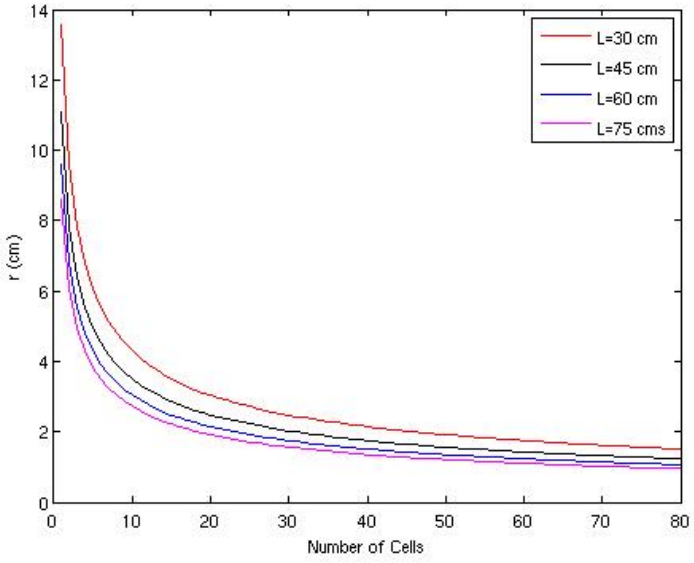

Figure 1.7. Cylindrical LT bed outside radius. Outside radius of a single LT bed cell for various cell lengths and for differing numbers of cells.

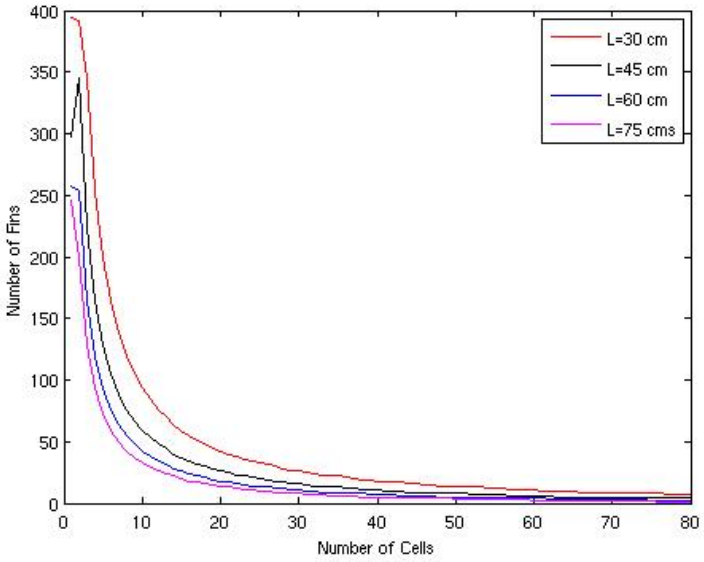

Figure 1.8. Cylindrical HT bed number of fins. Number of fins required on HT bed for various cell lengths and for differing numbers of cells.

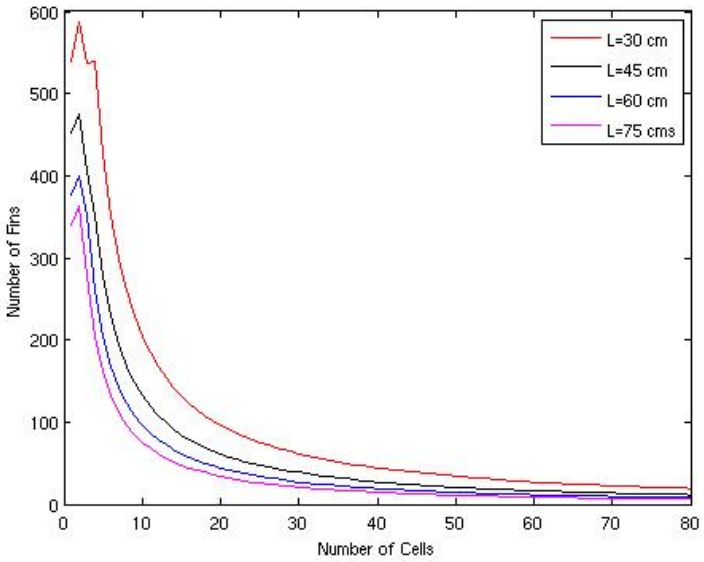

Figure 1.9. Cylindrical LT bed number of fins. Number of fins required on LT bed for various cell lengths and for differing numbers of cells.

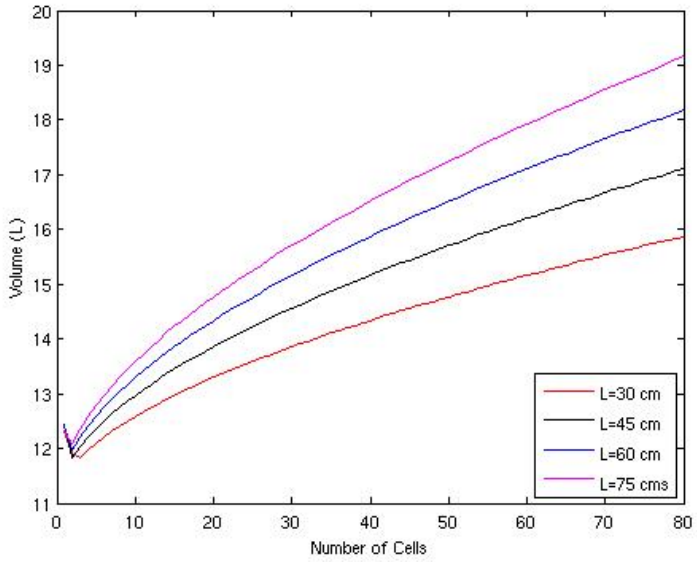

Figure 1.10. Cylindrical HT bed volume. Total volume of HT bed for various cell lengths and for differing numbers of cells.

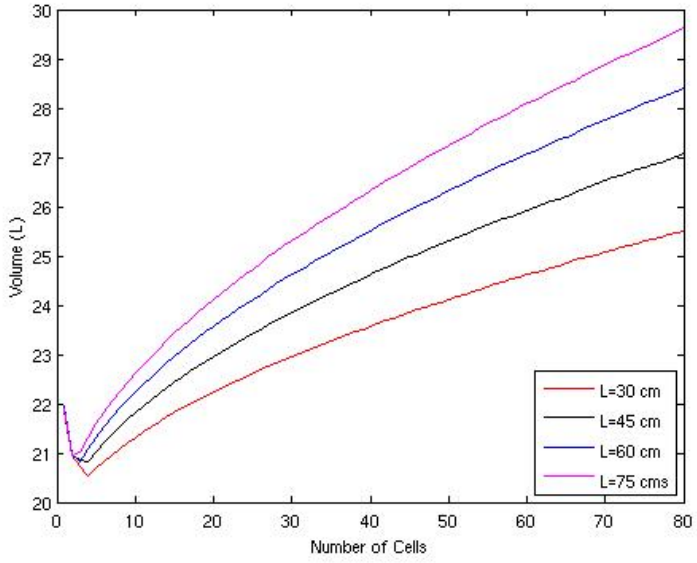

Figure 1.11. Cylindrical LT bed volume. Total volume of LT bed for various cell lengths and for differing numbers of cells.

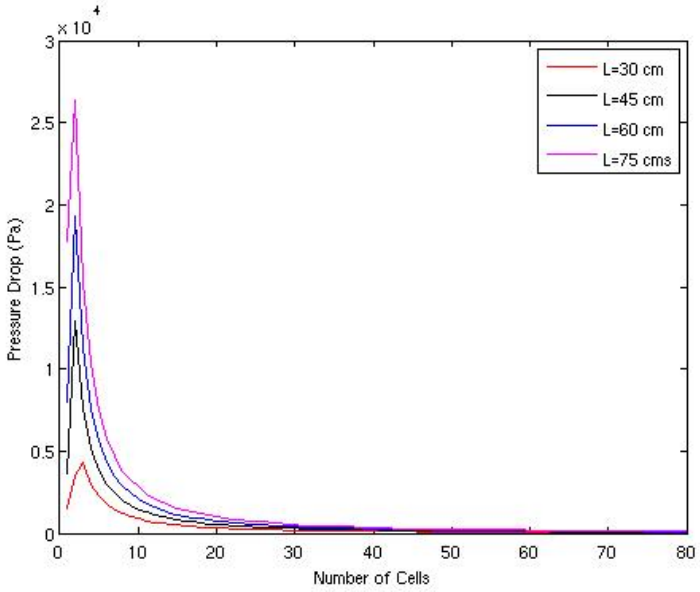

Figure 1.12. Cylindrical HT bed pressure drop. Air pressure drop along HT bed for various cell lengths and for differing numbers of cells.

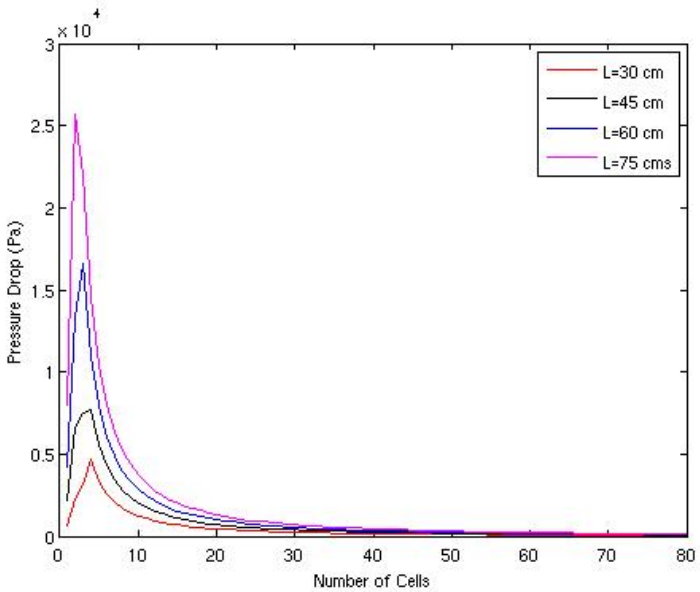

Figure 1.13. Cylindrical LT bed pressure drop. Air pressure drop along LT bed for various cell lengths and for differing numbers of cells.

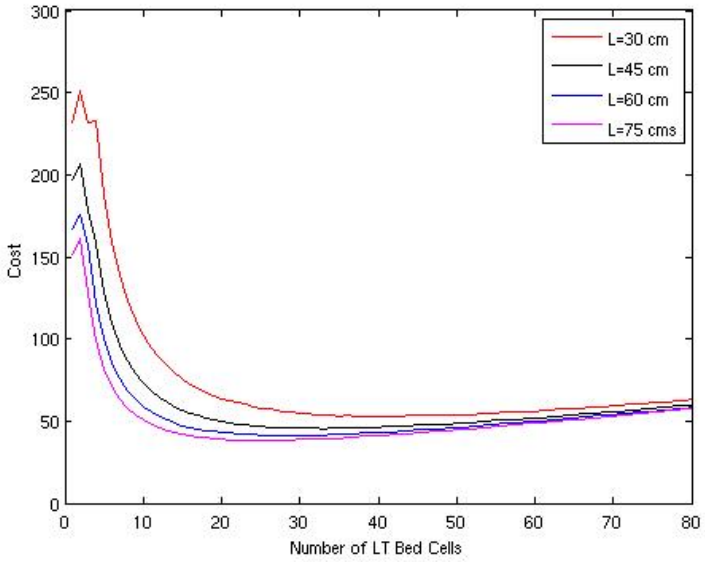

Figure 1.14. System cost as a function of the number of cold hydride cells.

Table 1.3. Metal hydride heat pump optimized design based on minimum cost.

bed	N	L (cm)	m (kg)	V (L)	r_{out} (cm)	t_w (mm)	ΔP (Pa)	n$_{fins}$	$E_{d,sys_{heat}}$ (kJ/kg)	η_{sys} (%)
HT	16	75	22.81	14.33	1.62	0.91	1357	18	225	62.3
LT	24	75	75.52	24.62	1.75	0.98	958	27		

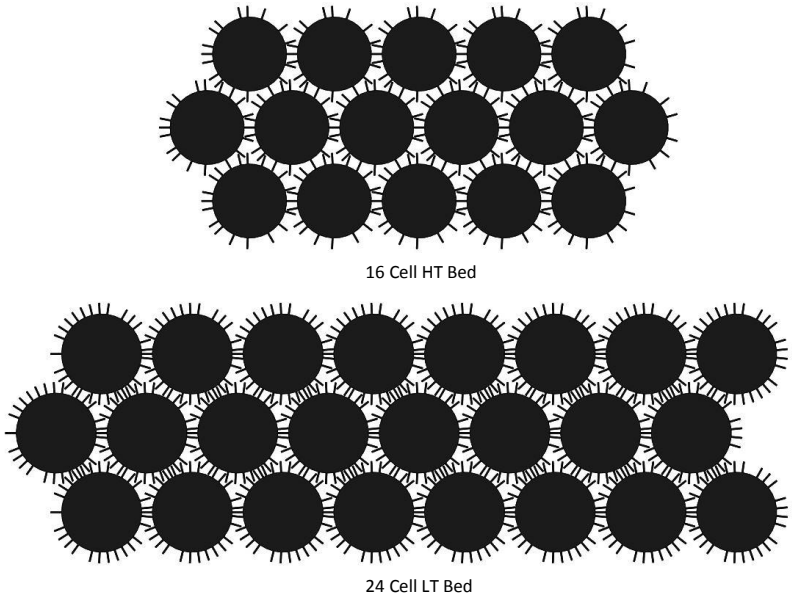

Figure 1.15. Potential arrangement for 24 cell LT bed with 27 fins and 16 cell HT bed with 18 fins. The arrangement of the fins represents one possible orientation in which there is no interference between fins and the cells are only one fin length apart. Additional orientations are possible and should be explored, though this model does not address optimal fin orientation.

CHAPTER 2

SYSTEM MODELING

There have been a number of studies reported in the literature that include models of metal hydride beds during hydrogenation and dehydrogenation reactions [16, 17, 18, 19, 20, 21, 22, 23].

Gambini developed an algorithm for the evaluation of metal hydride heat pumps under dynamic operation [16]. That mathematical algorithm was the basis for the model presented by Gambini, Manno and Vellini [17]. Their lumped capacitance model predicts hydride bed performance in a single bed system under constant pressure. The model was compared with previously reported experimental data with excellent agreement. Additionally, the system was modeled under other operating conditions to predict enhanced behavior.

Muthukumar, Singhal and Bansal analyzed the performance of a metal hydride hydrogen storage device with various internal cooling configurations [18]. A two-dimensional mathematical model was developed using COMSOL Multiphysics to simulate both the hydrogen absorption and the temperatures. The kinetics equations used in their model were similar to the equations proposed by Gambini.

Ahmed and Murthy proposed a novel three hydride system in which a hot, warm and cold bed were all operated simultaneously [19]. The performance of the cycle was modeled using a lumped capacitance model for each bed. The coefficient of performance for the system was also analyzed.

Additional simulations of metal hydrides using one-dimensional lumped capacitance models have been performed by numerous researchers [20, 21], along with other researchers proposing multidimensional models using computer software [22, 23].

In this work, the model of Gambini, Manno and Vellini [17] is modified to include the effect of a control valve between two beds. The hydrogen transfer between the beds is modeled using control valve theory to allow for design and optimization of a control system. The model is compared against the experimental results of a dual bed metal hydride thermal battery heat pump.

2.1 Lumped Capacitance Model Development

The objective of the lumped capacitance (LC) model is to predict the dynamic behavior of metal hydride thermal battery heat pumps. The model assumes that there are no radial or axial temperature variations. The purpose of the model is to quantify the performance of candidate hydrides for a given application, such as an electric vehicle climate control system or a heat recovery system.

In the paper presented by Gambini, Manno and Vellini [17] a detailed method for analyzing a single metal hydride bed was presented. That methodology is followed in this work and summarized below.

2.1.1 Kinetics

The first equation in defining the system is the reaction rate of the metal hydride to the presence of hydrogen. A widely accepted model for the reaction kinetics is used. This model allows for a pressure , a temperature and hydrogen concentration dependence on the reaction rate. The equation used is:

$$\frac{dX}{dt} = C_{a,d} \exp\left(\frac{-E_{a,d}}{RT}\right) ln\left(\frac{P}{P_{eq}}\right) |X - X_{lim}| \tag{2.1}$$

where $C_{a,d}$ is the pre-exponential coefficient, $E_{a,d}$ is the activation energy and X_{lim} is either 0 for a hydride undergoing desorption or X_{max} for a hydride under going absorption.

The equilibrium pressure of a metal hydride as a function of temperature is commonly defined using the Van't Hoff law:

$$\ln \frac{P_{eq}}{P_o} = \frac{\Delta H}{RT} - \frac{\Delta S}{R} \tag{2.2}$$

While this equation is useful in the plateau region it does not accurately predict the equilibrium pressure in the high and low concentration regions nor does it account for hysteresis in the metal or the slope of the plateau region. All of these elements can be seen in the sample PCT plot for $TiV_{0.62}Mn_{1.4}$ in Figure 2.1. To more accurately model the hydride in those regions a curve fit, in conjunction with the Van't Hoff law, is used:

$$\frac{P_{eq}}{P_o} = \exp\left[\frac{\Delta H}{R}\left(\frac{1}{T} - \frac{1}{T_{ref}}\right)\right] f \tag{2.3}$$

where P_o is usually defined as 1 bar and is often dropped from the equation, T_{ref} is the temperature at which the original PCT data is taken and the line fit is performed and ΔH is the enthalpy of absorption for the hydride. For example, if a line is fit to the absorption curve for 20 °C in Figure 2.1, then T_{ref} would be 293 K in equation 2.3.

Traditionally, a simple *nth* degree polynomial is used to fit a PCT curve and define the coefficient f, as shown in equation 2.4. If the line fit is unsatisfactory, as can occur for hydrides with low equilibrium pressures or flat plateau pressures, then a three part piecewise function should be used to model the low concentration region, plateau region and high concentration region, as shown in the sample PCT plot Figure 2.1.

$$f = \sum_{i=0}^{N} a_i X^i \tag{2.4}$$

2.1.2 Energy Balance

In order to model the temperatures of the two beds over time, the law of conservation of energy was used. Energy is stored in the bed by one of two means: 1) hydrogen absorbed in the metal hydride or, 2) thermal energy stored in the material. Including these modes of energy storage in the conservation of energy equation yields:

$$E = T\left(m_{MH}c_{P_{MH}} + m_C c_{P_C}\right) + \frac{\Delta H X}{M_{H_2}} b_x \tag{2.5}$$

Rearranging to solve for the temperature in the bed and taking the derivative with respect to time yields:

$$\frac{dT}{dt} = \left(\frac{-\Delta H}{M_{H_2}} b_x \frac{dX}{dt} + \frac{dE}{dt}\right) / \left(m_{MH}c_{P_{MH}} + m_C c_{P_C}\right) \tag{2.6}$$

where b_x is a conversion coefficient to change concentration from an atomic ratio to a hydrogen mass and $\frac{dE}{dt}$ is the rate of heat transfer to the environment. The equation for b_x is given in equation 2.7.

$$b_x = \frac{[MH] m_{MH}}{2} \frac{M_{H_2}}{M_{MH}} \tag{2.7}$$

The two in the denominator of equation 2.7 is the number of atoms per hydrogen molecule (H_2). This is used to convert the number of hydrogen atoms in the hydride to the number of moles of H_2 in the hydride.

The rate at which energy is taken from the system is very dependent on the design of the system. If the system is a heat exchanger with the cooling fluid inlet temperature and heat exchanger surface temperatures known, then equation 2.8 can be used. If the heat exchanger is exposed to convective and radiative heat transfer, where the inlet and outlet coolant temperatures are nearly the same, then equation 2.9 can be used. Equation 2.9 assumes that the emissivity of the surface and view factor to the surroundings are one and the surroundings are at the fluid inlet temperature.

$$\frac{dE}{dt} = \dot{m_f} c_{P_f} \epsilon (T_{f,in} - T) \tag{2.8}$$

$$\frac{dE}{dt} = hA_s \left(T_{f,in} - T\right) + \sigma \left(T_{f,in}^4 - T^4\right) \tag{2.9}$$

To calculate the heat exchanger efficiency(ϵ), the Number of Transfer Units (NTU) method is used where the efficiency is defined as:

$$\epsilon = 1 - \exp(-NTU) \tag{2.10}$$

The number of transfer units are defined as:

$$NTU = \frac{UA_s}{m_f c_{P_f}} \tag{2.11}$$

Finally, the overall heat transfer coefficient is defined as:

$$U = \left(\frac{1}{h} + \frac{r_e \ln r_e/r_i}{k_c} + \frac{r_e \ln r_i/r_m}{k_{MH}}\right)^{-1} \tag{2.12}$$

It should be noted that r_m is the distance to the where the temperature of the metal hydride bed is no longer nearly uniform. It should be chosen as a representative distance over which the bed temperature is decreasing and heat is being conducted. This term is used to account for the difference between the surface temperature and the metal hydride inner temperature. For metal hydrides with high conductivities, r_m will approach the distance to the center of the bed, indicating that conduction is happening along the entire radial length of the hydride bed. For metal hydrides with lower conductivity, r_m will approach the value of r_i, meaning that even very close to the surface, the metal hydride is incapable of efficient heat conduction.

2.1.3 Mass Balance

In order to calculate the rate of change in concentration, the free hydrogen pressure in the bed needs to be known. This pressure is calculated using the ideal gas law, $PV = mRT$, where m is the amount of free hydrogen inside of the bed. To calculate the pressure in the bed, the free mass of hydrogen at any given moment is needed.

For a single bed system being charged, the pressure in the bed is usually maintained at some constant pressure by a reserve tank. This makes it unnecessary to calculate the free hydrogen mass. If the rate of hydrogen mass entering the system from the reserve tank is desired, it is merely equal to the rate of hydrogen uptake, $dm/dt = b_x dX/dt$.

For a two bed system, the pressure in the bed is dependent on the amount of hydrogen in the bed at a given time. Because of this, a mass balance is performed for each bed. The

rate of change in concentration, dX/dt, is proportional to the amount of hydrogen released from or absorbed into the bed. The hydrogen then will either leave or enter the bed based on the pressure difference between the two beds. The mass balance for a given bed is shown below.

$$\frac{dm}{dt} = -b_x \frac{dX}{dt} - \dot{m}_{out} + \dot{m}_{in} \tag{2.13}$$

To calculate the rate of hydrogen leaving a bed, control valve theory was implemented [24]. By defining the mass flow through the valve in this manner, it allows for sophisticated control systems to be developed. While there will be many instances where the control valve specifications may not be known and approximate values will be sufficient, the control functionality allows the model to assist in the design of complex control systems for various applications.

Using manufacturer's specifications, a C_v and X_T can be defined. It is then necessary to determine if the flow through the valve will be sonic. When $P_r \geq 1.007 X_T$, where P_r is the pressure ratio defined as $P_r = (P_1 - P_2)/P_1$, the flow through the control valve is sonic. The subscript 1 denotes the bed with the higher pressure while subscript 2 denotes the bed with the lower pressure. For sonic flow, equation 2.14 should be used, while for subsonic flow, equation 2.15 should be used.

$$\dot{m} = 18.21 C_v \sqrt{1.007 X_T P_1 \rho_1} \tag{2.14}$$

$$\dot{m} = 27.3 C_v \left[1 - \frac{P_1 - P_2}{3.021 P_1 X_T}\right] \sqrt{(P_1 - P_2)\rho_1} \tag{2.15}$$

2.1.4 Initial and Boundary Conditions

With the equation for the kinetics, energy and hydrogen mass all defined, this system of three differential equations (2.1, 2.6, 2.13) can be solved. The initial and boundary conditions that need to be defined are: coolant inlet temperature ($T_{f,in}$), the initial hydrogen concentration for both beds ($X_{o,LT,HT}$) and the initial bed temperature ($T_{o,LT,HT}$).

To solve the system, a fourth order Runge-Kutta differential equation integrator was implemented with a time step of 10 ms. For dual bed systems, the set of differential equations has found to be a "stiff" system and can lead to significant errors if sufficiently small time steps are not used, resulting in long computation time. For dual bed analysis it is recommended to use a solver specifically designed for stiff differential problems.

2.2 Single Bed Validation - $MmNi_{4.6}Fe_{0.4}$

To validate the LC model, the model output was first compared against data published by Muthukumar et al. [25], as performed by Gambini et al. [17].

2.2.1 Setup

The device consists of a cylindrical cell filled with the metal hydride $MmNi_{4.6}Fe_{0.4}$. Additionally, eight copper fins are installed inside of the cell to improve the thermal conductivity of the bed. The cell is made out of stainless steel. Around the exterior of the cell, water is pumped at a specified flow rate to act as a cooling liquid. The water is maintained at a fixed temperature by using a thermostatic bath and a fixed flow rate to provide a set heat transfer rate. Additional information about the setup can be found in the original paper. A schematic of the experimental setup is given in the papers by both [25] and [17].

2.2.2 System Properties

The material properties for stainless steel and copper can readily be found in online or published texts. These values are listed in Table 2.1.

It should be noted that the thermal conductivity of copper is not reported. This is due to the fact that the copper is acting as an enhancement of the thermal conductivity of the metal hydride and is lumped in with that value.

The material and kinetic properties for the metal hydride are reported in Table 2.2. These values were taken from either the paper published by Gambini et al. or were found by identification with the experimental data. It is important to note that the thermal conductivity reported below differs from the value reported Gambini. This may be due to the fact that in the model performed by Gambini the thermal capacitance of the copper is neglected while in the modeling performed here, the thermal capacitance of copper is taken into account.

In addition to the data contained in Table 2.2, the equilibrium pressure at various temperatures needs to modeled using equation 2.3 and 2.4. To do this the coefficients reported by Askri et al. [23] were used. These values were used because they most closely matched the data reported by Muthukumar et al. These coefficients are reported in Table 2.3.

The convective heat transfer rate can be determined from the overall heat transfer coefficient reported in [25]. It is stated that the overall heat transfer coefficient for the

stainless steel shell and coolant at a volumetric flow rate of 2.1 L/min is 1000 W/m^2. Using the relationship:

$$\frac{1}{U} = \frac{1}{h} + \frac{r_{out}\ln(r_{out}/r_{in})}{k_{ss}} \tag{2.16}$$

the convective heat transfer coefficient can be found to be h = 1257 W/m^2-K.

Finally, the mass of copper and stainless steel was determined by calculating the volume from dimensions reported in [25] and using the density reported in Table 2.1. It was found that the mass of the stainless steel was approximately 1.0 kg and the mass of the copper was approximately 0.5 kg. The mass of the metal hydride was given in the original paper as 0.5 kg.

2.2.3 Results

With all of the system, material and kinetic properties defined, it is now possible to model the system and compare it to the reported data. Figures 2.2 and 2.3 show such a comparison.

Figure 2.2 demonstrates that the LC model has the ability to accurately predict the hydride temperature under constant hydrogen pressure. Figure 2.3 demonstrates that the model has the ability to predict hydrogenation kinetics at various hydrogen pressures. While there is some error between the numerical and experimental data, the predictions match the reported data quite well. It is not clear whether the discrepancies between the experimental and numerical data are due to experimental issues or minor deficiencies inherent in the use of the LC method.

In addition to the match of the model to the data published by Muthukumar et al., the model duplicates the results reported by Gambini et al.

2.3 Single Bed Validation - $LaNi_5$

A second single bed analysis was performed using the LC model to further validate its use. The experiment was developed and performed in the Sustainable Energy Lab of the Mechanical Engineering department at the University of Utah.

2.3.1 Setup

The metal hydride bed is shown in Figure 2.4. The device consists of a cylindrical cell filled with the metal hydride $LaNi_5$. Inside of the bed, three eleven point thermocouple probes are inserted at different radial distances. A pressure transducer is installed on both the hydrogen inlet and outlet, allowing for an average bed pressure to be calculated along

the length of the bed. Hydrogen is allowed to enter the bed at a constant pressure from a regulated tank. The hydrogen outlet tube is closed to prevent any hydrogen from escaping the vessel. The vessel and its components are made out of stainless steel 316L. A cut, top and bottom view are shown in Figures 2.5 to 2.7, respectively.

Before the experiment is run, the bed is evacuated using a scroll type vacuum pump to remove all hydrogen from the bed. The bed is then allowed to come to equilibrium temperature. The corresponding temperature and pressure at equilibrium are used to determine the initial hydrogen concentration.

The center tube in Figure 2.5 is for the insertion of a heating cartridge. This allows for the heating of the bed during evacuation to improve the desorption kinetics and shorten the desorption time.

The diffuser, which is for the uniform distribution of hydrogen at the inlet, and the piston both have two micron nominal mesh screens installed. This mesh is to prevent the metal hydride powder escaping the testing chamber and getting into the hydrogen lines.

The spring and piston at the bottom of the cell are to account for the expansion and contraction of the metal hydride. When a metal hydride absorbs hydrogen, its molecular structure changes and the specific volume of the material increase. To ensure that the metal hydride does not settle, the piston spring system was installed to provide gentle pressure, keeping the metal hydride compact. This was necessary because the system operates horizontally, as opposed to vertically like many metal hydride test stations.

2.3.2 System Properties

The properties for the vessel material are previously reported in Table 2.1. The properties for the $LaNi_5$ are widely available in various publication as the material has been highly studied [26, 27, 12]. The properties used are shown in Table 2.4.

During the experiment, the bed was maintained at a constant six bar pressure. This pressure was set at the hydrogen tank outlet and verified using the two installed pressure transducers.

To improve the absorption kinetics, a fan was blown across the bed. The purpose for using the fan was to improve heat transfer and decrease the charging time. The fan was oriented in a cross flow direction. The convective heat transfer coefficient was determined by matching with the experimental data. The value used is h = 15 W/m^2-K.

The equilibrium pressure data for $LaNi_5$ from the published data [28] were difficult to fit using a polynomial due to the very flat plateau region of the PCT plot. To better model

the PCT, a piecewise function was used for the coefficient f in equation 2.3. That function is given in equation 2.17.

$$f = \begin{cases} 4512.9X^3 - 1599X^2 + 186.1X - 4.89, & \text{if } X < 0.1 \\ 0.398X + 2.16, & \text{if } 0.1 \leq X \leq 0.92 \\ 1183.6X^3 - 3166.2X^2 + 2823.1X - 836.5, & \text{if} X > 0.92 \end{cases} \tag{2.17}$$

It should also be noted that in this experiment, the effect of radiative heat transfer is taken into account. In the last experiment (sec. 2.2), the effects of radiation were neglected due to the high convective heat transfer coefficient. In this experiment the convection term is much lower, allowing for radiation to have a larger affect. To account for this, equation 2.9 was used to model the loss of energy from the system.

Finally, the mass of the metal hydride was measured to be 1.212 kg. The mass of the portion of the stainless steel containment vessel that is thermally active is difficult to assess due to the low thermal conductivity of the metal hydride, the complexity of the structure and the changing length of the chamber due to the expansion and contraction of the metal hydride. An effective mass of 0.5 kg was estimated to be representative of the thermally active portion of the vessel.

2.3.3 Results

Figure 2.8 show the temperatures predicted by the LC model compared to the experimental data. Figure 2.9 shows the predicted concentration of the bed over time.

As can be seen in Figure 2.8, the temperature of the bed matches closely to the experimental data during the decay period, but does not reach the same maximum temperature. This could be due to a number of things such as: the value used for ΔH is too high resulting in slower kinetics and a higher equilibrium pressure, the model used to predict the equilibrium pressure at elevated temperatures overestimates the pressure for $LaNi_5$, or the experimental average temperature is too high since it is based solely on internal temperatures from the thermocouple probes and does not account for the temperatures near the surface which are much cooler. Even with the larger error at the initial charging, the relative error of the model is at the most only 6%. Considering that the thermocouple probes themselves have a margin of error of +/-2.2 °C, the error between the numerical and the experimental data is quite small.

Figure 2.9 shows the average concentration of the hydride over time. This figure is about what is expected. With the decay in temperature being linear, and since the heat transfer coefficient is constant, the rate of heat addition (hydrogen absorption) must also be

constant. This is easily seen in the figure since the concentration increases in a linear fashion after the initial opening of the valve. If the experiment was continued it would be expected that the concentration would begin to asymptote as it approaches its concentration limit and the temperature would begin to decrease in a nonlinear fashion.

2.4 Two Bed Validation

To verify the ability of the LC model to simulate a two bed system operating in heat pump mode, another experiment was performed. This experiment was developed in the Metallurgical Engineering department at the University of Utah. It was originally developed as a proof of concept demonstration of a metal hydride thermal battery energy storage device but was also used to validate the model developed in this chapter.

2.4.1 Setup

The system consisted of two tubes, one containing a cold hydride and the other containing a hot hydride. A cross-sectional view of one of the tubes is shown in Figure 2.10.

The LT and HT cells were identical. The amount of hydride in each tube was different based on the density of the hydride.

The HT bed was prepared by evacuating the hot hydride for about 3 hours at a constant temperature of 280 °C. The LT bed was prepared by connecting the bed to high pressure hydrogen of about 30 bar. The bed was cooled with a fan and allowed to come to room temperature. Once the bed was at room temperature with the pressure still at 30 bar, the bed was assumed to be fully charged.

The initial pressure in the cold bed is measured along with initial temperatures in both beds. The bed temperatures are measured on the surface using a thermal imaging camera mounted on a tripod. With the camera, an average bed temperature is calculated every 15 seconds.

2.4.2 System Properties

The metal hydrides used in the system are $TiV_{0.62}Mn_{1.4}$ for the LT hydride and Mg doped with TiH_2 for the HT hydride. The properties for $TiV_{0.62}Mn_{1.4}$ are available as this hydride has previously been studied [12]. The $MgH_2{-}0.1TiH_2$ hydride was developed and studied recently and the necessary values were found in the published literature for this study [11]. Additional values were provided under collaboration with the Metallurgical Engineering department at the University of Utah.

A summary of all the values used for both materials is shown in Table 2.5.

The equilibrium pressure for the LT bed was found to be best fit by a 13th order polynomial. The values for the polynomial can be found in the Table 2.6. The original data were provided by the manufacturer and are shown in Figure 2.1.

The equilibrium pressure for the HT bed was found to be best fit by a 13th order polynomial. The values for the polynomial are found in Table 2.7. The data for the line fit was found in the originally published paper by Lu et al. [11].

During the experiment, there was no cooling system installed so only free convection and radiation are considered. Free convection is traditionally in the range of 2-25 W/m^2-K [29]. The value used for this model was found to be 2 W/m^2-K.

Since this system is connected together by a control valve, equation 2.13 will be used. It is necessary to define the C_v and X_T values for the valve used in order to model the hydrogen flow. The X_T value is dependent on the type of valve being used. The valve employed is a simple ball valve with an X_T value of 0.7. The C_v value is determined by the manufacturer and how open the valve is. Unfortunately, there was no C_v value reported by the manufacturer so an approximation had to be made. In this experiment the valve was completely opened. Since the pressure difference between the two beds was so high and the amount of hydrogen was relatively small, the value used for C_v was found to not significantly change the results as long as its value was above a minimum of 1. A value of 100 was used in the analysis.

The mass of the metal hydrides were roughly measured when installed in the system. The reported mass of the HT bed was 50 g and the LT bed was 200 g. Both beds were reported as being plus or minus 5 g. Best matches between the model and the data were found when 205 g and 45 g were used in the model for the LT and HT beds, respectively. Additionally, since the volume the metal hydride occupies will be different for each bed, the mass of the stainless steel for each bed will be slightly different. The mass of stainless steel for the HT bed was estimated to be 0.44 kg and the mass for the LT bed was estimated to be 0.6 kg based on approximations of material volume.

2.4.3 Results

Figure 2.11 shows the results of the LC model and the experimentally determined average bed temperatures for both the HT and LT beds. Figure 2.12 shows the calculated bed pressure and the experimentally determined bed pressure.

As can be seen in Figure 2.11, the LC model is able to predict the bed temperatures with some accuracy. The predicted temperatures of the LT bed more accurately reflect the data than those for the HT bed. Additionally, for the HT bed, there is some sort of

phenomenon occurring around the 200 second mark that drastically increases the average temperature, but then quickly disappears and slows down.

2.4.4 Discussion

When analyzing the results of the LC model, the first thing that must be understood is that this station was designed for demonstration purposes and not for experiments. Because of that, the system was put together quickly and all of the necessary instrumentation was not included. The only pressure measurement available was on the LT bed. It can only be assumed that the HT bed had a similar pressure. Also, without an initial pressure of the HT bed, the initial concentration must be matched to the data. Additionally, there are no temperature measurements made on the inside of the cylinder. This means that only surface temperature measurements can be made and the internal temperature must be calculated based on the thermal conductivity of the metal hydride.

It was also found that there was a slow leak of air into the HT bed due to the vessel not being air tight. Exposure of the metal hydride to air leads to contamination of the material, and the inability to uptake hydrogen. To prevent contamination, the HT bed was charged with argon when not in use. This most likely extended the life of the system, but not long after this experiment was performed the bed was deemed fully contaminated and incapable of functioning. This leads to an important question about the properties of the $MgH_2{-}0.1TiH_2$ hydride.

To match the experimental results with the model, it was found that the concentration limit (X_{max}) needed to be changed. To account for the contamination of the hydride, the concentration limit was adjusted downward to 0.71.

At the end of the experiment, when the HT bed had stopped heating up and the pressure had leveled out, the numerical and experimental pressures were nearly identical. This indicates that the concentration and temperature predicted by the model closely match what was found experimentally. This seems to validate the idea that the maximum concentration of the HT bed was indeed reduced to the level suggested earlier as a result of bed contamination.

It is unclear whether the additional error is due to deficiencies in the LC model, inaccuracies in the material properties or experimental phenomenon that are occurring that the LC model cannot predict. These phenomenon include, but are not limited to, shifting powder that can block hydrogen flow, hydrogen blockage at the inlet or inert powder due to contamination.

Based on the correlation between the LC model and experimental data in the three separate experiments, two important conclusions are reached about the model accuracy: 1) the LC model is most accurate for single cell systems being charged under constant pressure and 2) the LC model has the highest accuracy for metal hydrides with relatively higher thermal conductivities.

2.5 Conclusion

Through comparisons with the separate data sets, it was found that the LC model has the ability to predict the average temperature histories of metal hydride beds with reasonable accuracy. It was also shown that it can predict the concentration of the metal hydride bed throughout the hydrogenation process.

Limits to the LC model were also found. The model requires extensive knowledge about the metal hydride, the geometry and the heat transfer rates. It requires some approximations to be made about heat transfer surfaces and container mass. The temperature provided are average temperatures, which mean localized hot spots or cold spots are not considered.

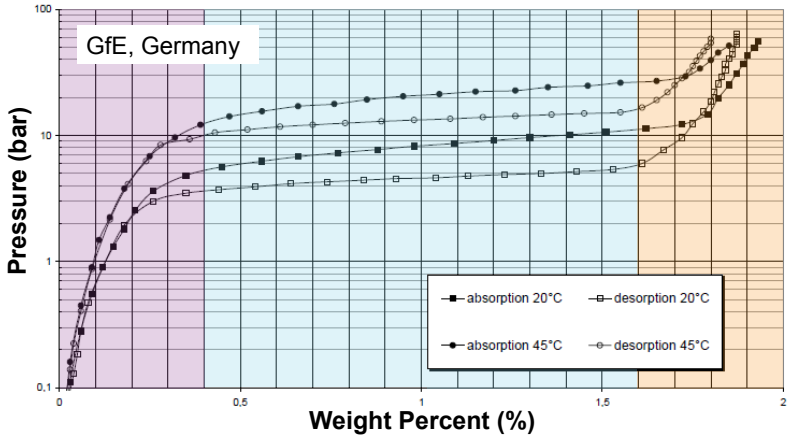

Figure 2.1. Sample PCT plot for $TiV_{0.62}Mn_{1.4}$. PCT plot provided by manufacturer (GfE, Germany). The purple area of the plot indicates the region of low concentration, the blue area indicates the plateau region and the orange area indicates the region of high concentration.

Table 2.1. Material properties for stainless steel and copper.

	Density (kg/m^3)	c_p (J/kg-K)	k (W/m-K)
Stainless Steel	7860	500	16.2
Copper	8960	390	-

Table 2.2. Material and kinetic properties for $MmNi_{4.6}Fe_{0.4}$.

	X_{max}	ΔH (J/mol H_2)	$E_{a,d}$ (J/Mol H_2-K)	$C_{a,d}$ (1/sec)	c_p (J/kg-K)	k (W/m-K)
$MmNi_{4.6}Fe_{0.4}$	1.2	-23000	25000	500	350	7

Table 2.3. $MmNi_{4.6}Fe_{0.4}$ equilibrium pressure coefficients at T_{ref} =298 K.

a_0	a_1	a_2	a_3	a_4
1.086	291.262	-2471.83	13076.3	-42253.8
a_5	a_6	a_7	a_8	a_9
85214.4	-107983	83863.7	-36592	6887.85

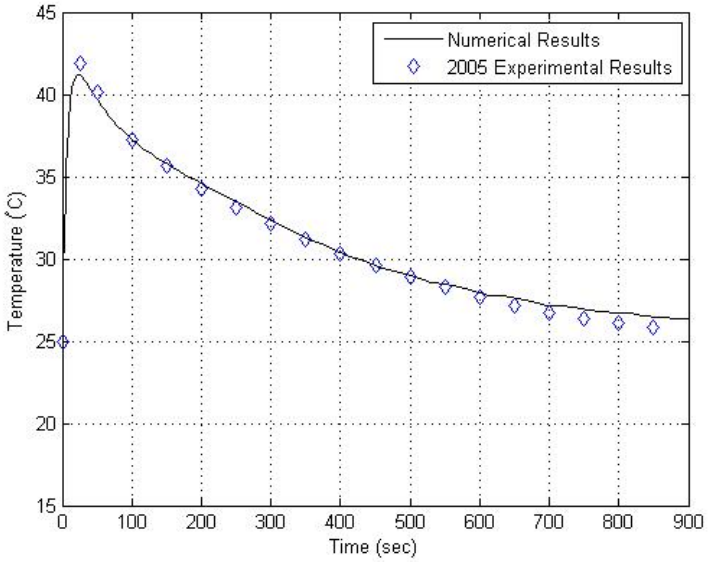

Figure 2.2. Single bed temperatures for $MmNi_{4.6}Fe_{0.4}$. Bed temperature over time comparison between reported values in [25] and numerical data calculated by the LC model for absorption at constant pressure (P=35 bar) and constant coolant flow rate ($V_{coolant}$=2.1 L/min).

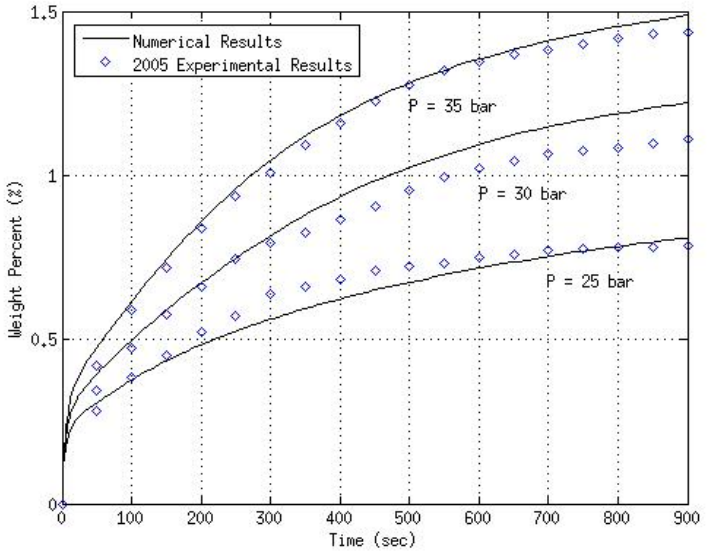

Figure 2.3. Single bed weight percent for $MmNi_{4.6}Fe_{0.4}$. Weight percent over time comparison between reported values in [25] and numerical data calculated by the LC model for absorption at three different hydrogen pressures and constant coolant flow rate ($V_{coolant}$=2.1 L/min).

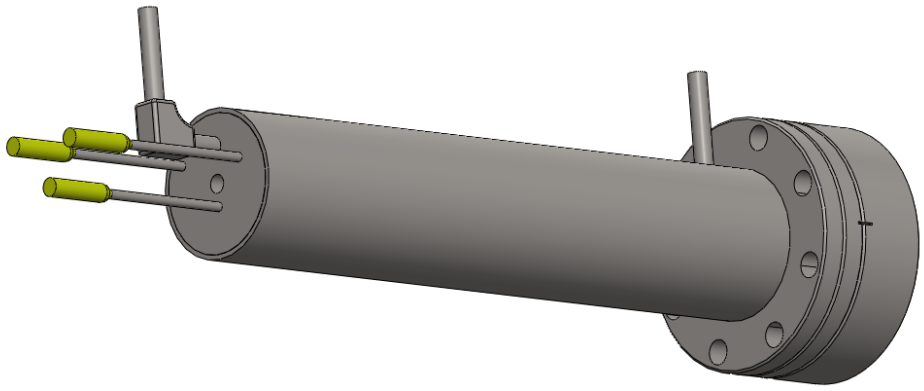

Figure 2.4. Isometric view single of bed experimental setup with $LaNi_5$.

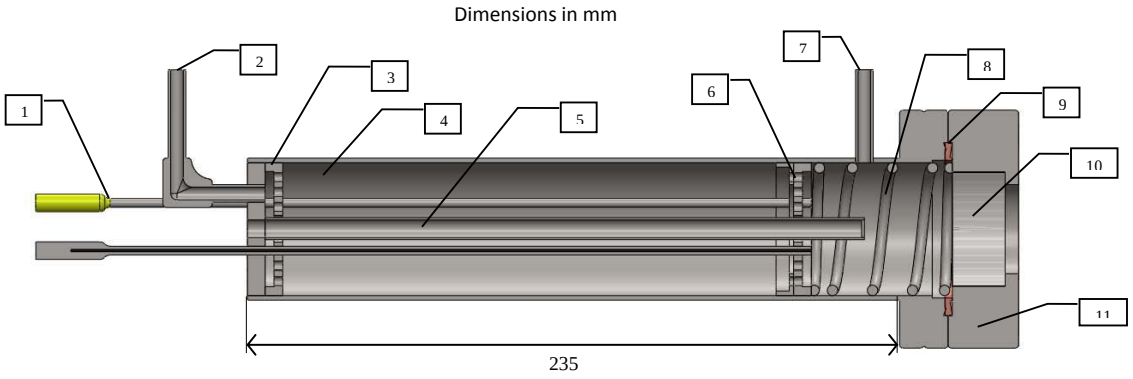

1. 11 Point Thermocouple Probe
2. Hydrogen Inlet
3. Diffuser
4. Metal Hydride
5. Heating Cartridge
6. Piston
7. Hydrogen Outlet
8. Spring
9. Copper O-ring
10. Sapphire Viewport
11. Flange

Figure 2.5. Cut view of single bed experimental setup with $LaNi_5$.

Table 2.4. Material and kinetic properties for $LaNi_5$.

	X_{max}	ΔH (J/mol H_2)	$E_{a,d}$ (J/Mol H_2-K)	$C_{a,d}$ (1/sec)	c_p (J/kg-K)	k (W/m-K)
$LaNi_5$	1.08	-30000	27700	45	419	0.9

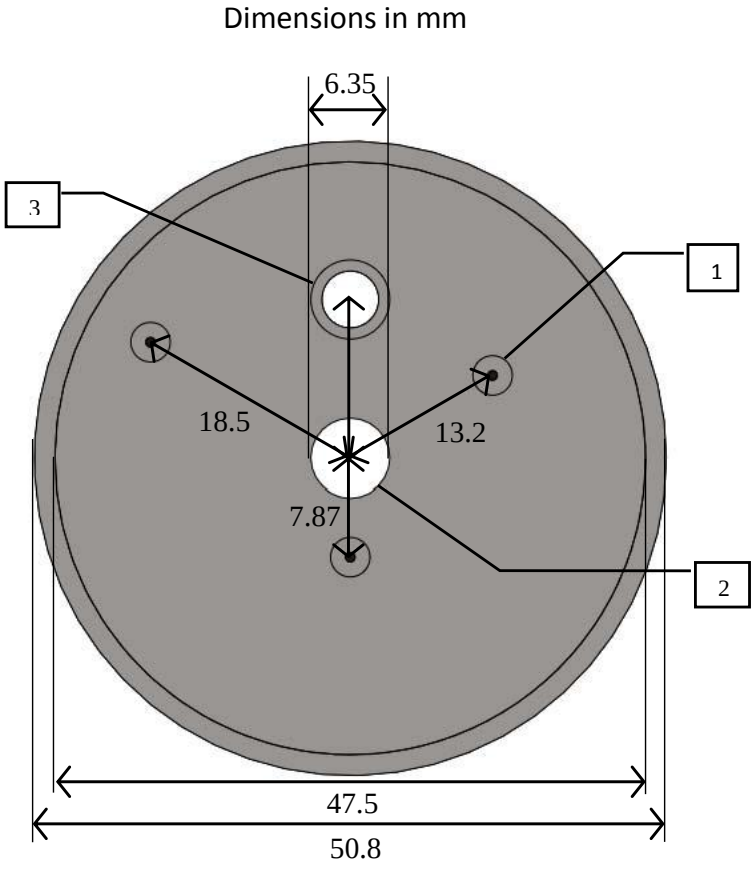

1. 11 Point Thermocouple Probe
2. Heating Cartridge Access
3. Hydrogen Inlet

Figure 2.6. Top view of single bed experimental setup with $LaNi_5$.

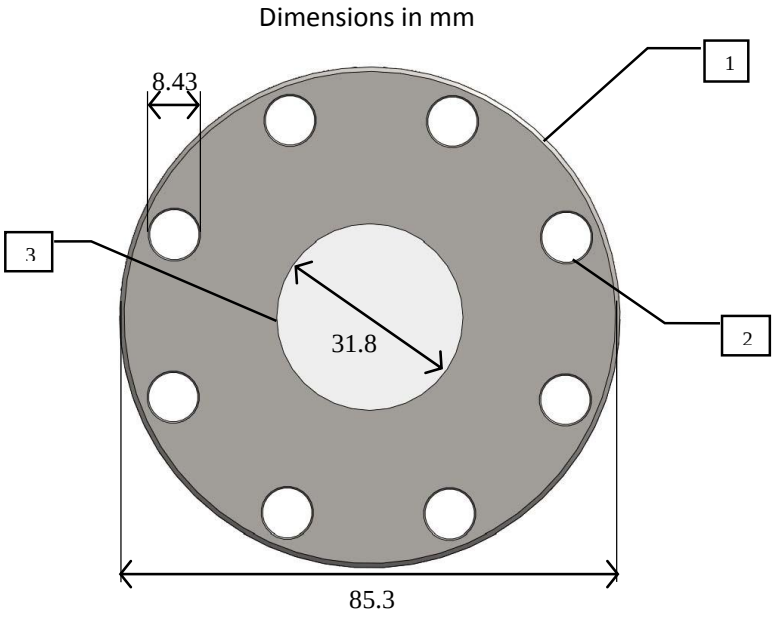

1. Pressure Chamber Flange
2. Bolt Hole
3. Sapphire Viewport

Figure 2.7. Bottom view of single bed experimental setup with $LaNi_5$.

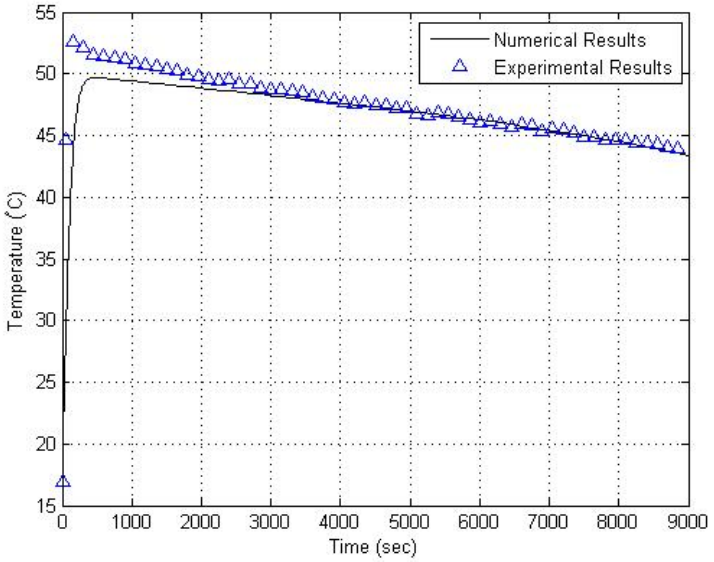

Figure 2.8. Single bed temperatures for $LaNi_5$. Bed temperature over time comparison between experimental values and numerical data calculated by LC model for absorption at constant pressure (P=6 bar) and constant convective cooling rate (h = 15 W/m^2-K).

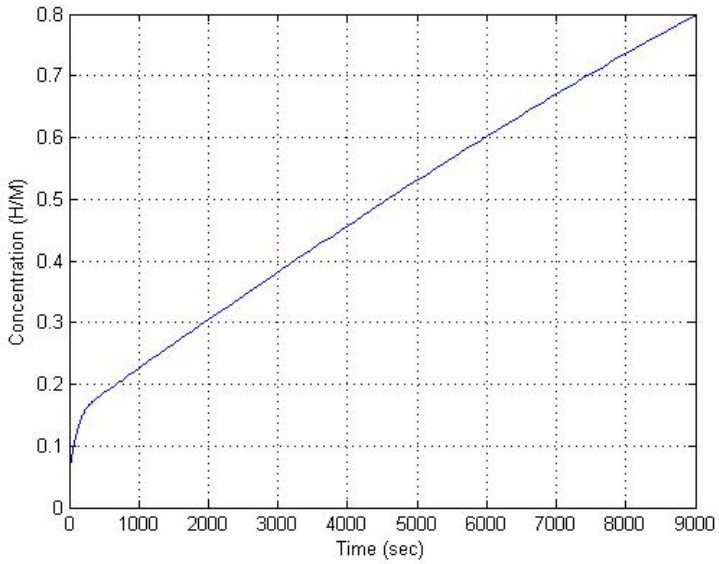

Figure 2.9. Single bed concentration for $LaNi_5$. Concentration over time numerical data as calculated using the LC method.

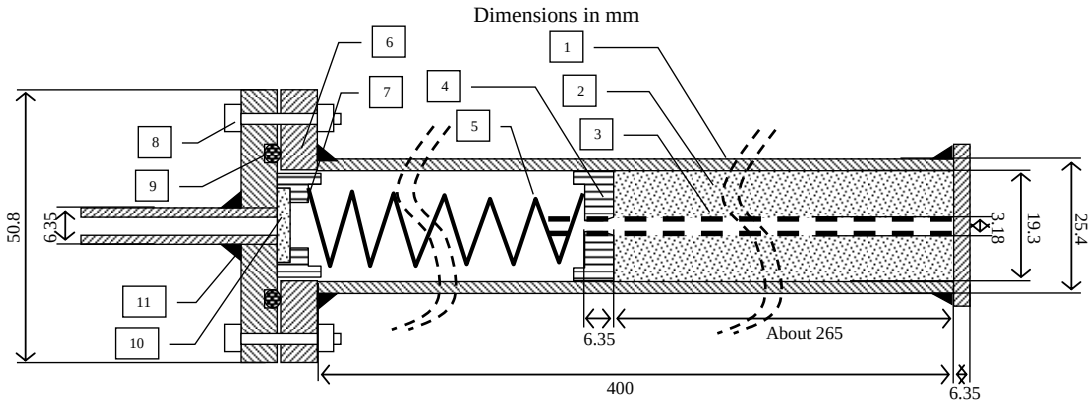

1. Stainless Steel Tube
2. Metal Hydride Powder
3. Stainless Steel Filter Tube
4. Stainless Steel Piston
5. Steel Spring
6. Stainless Steel Flange
7. Stainless Steel Support
8. Bolt
9. Silicone Rubber O-ring
10. Filter
11. Weld

Figure 2.10. Two bed experimental setup. Cross-sectional view of one tube from two bed experiment. In the experiment both beds were identical in design.

Table 2.5. Material and kinetic properties for $MgH_2{-}0.1TiH_2$ and $TiV_{0.62}Mn_{1.4}$.

	X_{max}	ΔH (J/mol H_2)	$E_{a,d}$ (J/Mol H_2-K)	$C_{a,d}$ (1/sec)	c_p (J/kg-K)	k (W/m-K)
$MgH_2{-}0.1TiH_2$	1.6	-68200	34500	115	385	0.15
$TiV_{0.62}Mn_{1.4}$	1.14	-28600	20000	30	500	0.25

Table 2.6. $TiV_{0.62}Mn_{1.4}$ equilibrium pressure coefficients at $T_{ref} = 20°C$.

a0	a1	a2	a3	a4
-0.287849	40.4713934	-1341.3051	27486.4415	-237293.94
a5	a6	a7	a8	a9
1017988.63	-1911325.7	-1417805.1	16157538.6	-39769305
a10	a11	a12	a13	
52698929.7	-40786308	17382481.4	-3161009.6	

Table 2.7. $MgH_2-0.1TiH_2$ equilibrium pressure coefficients at $T_{ref} = 240°C$.

a0	a1	a2	a3	a4
-0.0031547	11.1225305	-249.68581	2942.33973	-18143.618
a5	a6	a7	a8	a9
66481.4954	-156655.9	248127.11	-269813.99	201932.179
a10	a11	a12	a13	
-102228.4	33434.9828	-6375.0108	538.119986	

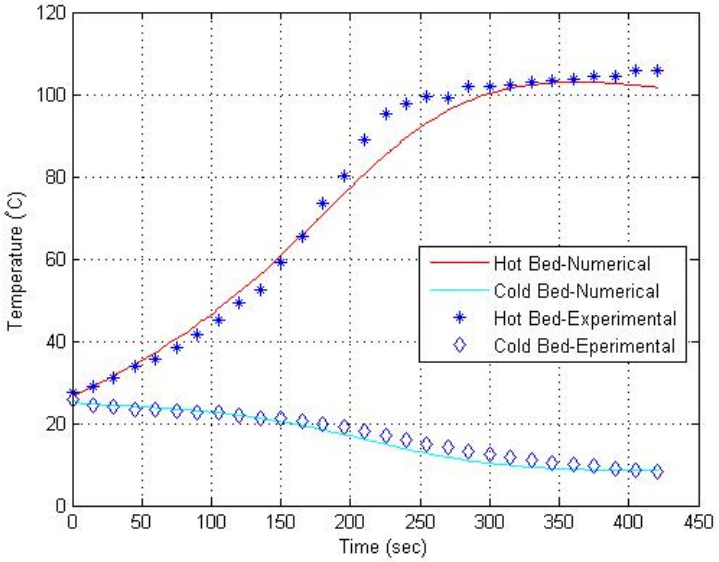

Figure 2.11. Two bed temperatures. Bed temperature over time comparison between experimental values and numerical data calculated by the LC model for a two bed system operating in heat pump mode.

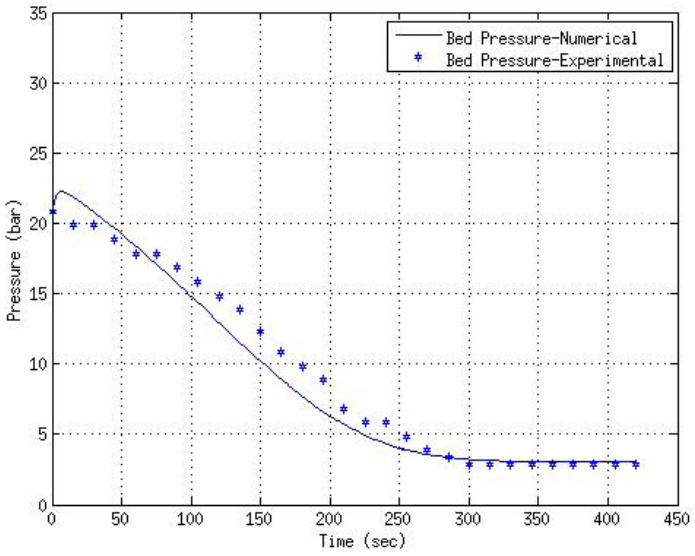

Figure 2.12. Two bed pressure. Bed pressure over time comparison between experimental values and numerical data calculated by the LC model for a two bed system operating in heat pump mode.

CHAPTER 3

KINETIC TEMPERATURE DEPENDENCE AND LUMPED CAPACITANCE LIMITATIONS

Lumped capacitance (LC) models for heating and cooling of metal hydrides during hydrogenation and dehydrogenation processes, similar to the one developed in the previous section, have been widely used for many years [16]. However, the validity of the model has not been assessed except for comparisons against experimental data. While the experimental data are useful for verifying the applicability of a model to a specific bed geometry and material, they do not guarantee that the model is also valid for other configurations and metal hydrides. In the following sections, the validity of the LC model will be analyzed, a criterion is developed to help determine when the temperature variation in the hydride can be neglected.

3.1 Traditional Lumped Capacitance

In a traditional LC analysis, the temperature within the material is assumed to be uniform, so when the material experiences a sudden change in the temperature of its surroundings, the temperature between the material's surface and the surroundings is much larger than any within the material. A common example is that of a hot piece of metal being cooled in air. The validity of the LC model is dependent on the following criteria [29]:

$$Bi = \frac{hL_c}{k} < 0.1 \tag{3.1}$$

where Bi is the Biot number, h is the convective heat transfer coefficient, k is the thermal conductivity of the hydride and L_c is the characteristic length defined as $L_c = V/A_s$. A more conservative approach would be to define the characteristic length as the dimension of the region experiencing the maximum temperature gradient. For a long cylinder the characteristic length is just the radius divided by 2.

The Biot number for three of the hydrides analyzed is presented in Table 3.1 for the actual experimental setup along with three additional radii. The first L_c entry listed for each metal hydride in Table 3.1 is the characteristic length for the experimental setup. Note that the characteristic length for the actual setup is defined using the relationship $L_c = V/A_s$ since there is an internal tube in each experiment.

It is apparent that for heat transfer coefficients in the range of most applications ($h >$ 20W/m^2-K) the Biot number will likely be greater than 0.1, except for $MmNi_{4.6}Fe_{0.4}$ which has had its thermal conductivity enhanced with copper fins imbedded in hydride bed. Even with the enhanced thermal conductivity for $MmNi_{4.6}Fe_{0.4}$, for the heat transfer coefficient of the published experiment [25](h = 1257 W/m^2-K), the Biot number would be greater than 0.1. Based on the conventional criteria, the LC technique would not be a valid method of evaluation for any of the experiments performed in the previous chapter.

In a simple LC transient heating or cooling problem the relative effects of convection and conduction, the relationship that the Biot number represents, are responsible for the temperature difference within the material. For a metal hydride experiencing a change in hydrogen pressure though, the major contributor in the temperature difference within the material is the heat generation during hydrogen absorption. Since heat generation is not taken into account in traditional LC heat transfer analysis, the Biot number does not provide a complete criteria for deciding whether or not the LC model is valid.

3.2 Volumetric Heat Generation

As previously mentioned, when a hydride is in the presence of high pressure hydrogen, it has the ability to absorb the hydrogen and release a large amount of energy. This energy is manifested as heat and the temperature of the metal hydride rises. The rate at which the metal hydride is absorbing or desorbing hydrogen is the controlling factor for the bed temperature.

As hydrogen is introduced into a metal hydride bed and permeates the gas voids, heat generation occurs throughout the entire bed. For uniform gas pressure and uniform distribution of hydride powder, the temperature change with time would be uniform within the bed. However, if the surface of the bed is cooled, the induced temperature gradient might invalidate the Biot number criterion or produce nonuniform heat generation rates due to the temperature dependence of the absorption and desorption kinetics of the hydride.

3.2.1 Temperature and Pressure Dependence of Absorption Kinetics

The first step in understanding the effect of the volumetric heat generation on the validity of the LC model, is to analyze the effect that temperature and pressure have on absorption and desorption rates.

From equations 2.1 and 2.3 it can be seen that the temperature of the bed affects both the exponential term as well as the logarithmic term in the kinetics equations while pressure only contributes to the logarithmic term. If these two equations are combined, equation 3.2 can be dervied:

$$\frac{dX}{dt} = C_a \exp\left(\frac{-E_a}{RT}\right) \ln\left(\frac{P}{P_o \exp\left[\frac{\Delta H}{R}\left(\frac{1}{T} - \frac{1}{T_{ref}}\right)\right] f}\right) |X - X_{lim}| \tag{3.2}$$

Rearranging the equation so that all of the terms with a temperature and pressure dependence are on the right and the other terms are on the left and calling the left hand side Y, yields:

$$Y = \exp\left(\frac{-E_a}{RT}\right) \ln\left(\frac{P}{P_o \exp\left[\frac{\Delta H}{R}\left(\frac{1}{T} - \frac{1}{T_{ref}}\right)\right] f}\right) \tag{3.3}$$

This term represents the portion of the metal hydride kinetics equation that is temperature and pressure dependent. If we assume that the metal hydride is in the plateau region on its PCT plot, then the equilibrium pressure can be defined using equation 2.2 instead of 2.3. This then leads to Y being defined as:

$$Y = \exp\left(\frac{-E_a}{RT}\right) \left[\ln\frac{P}{P_o} - \left(\frac{\Delta H}{RT} - \frac{\Delta S}{R}\right)\right] \tag{3.4}$$

This equation allows for a temperature and pressure kinetics dependence analysis that is independent of concentration.

Figures 3.1 to 3.3 show the temperature and pressure dependence of the kinetics of three metal hydrides considered in this study at a concentration within the plateau region of their PCT plots.

The dotted line in Figures 3.1 to 3.3 identifies the maximum absorption rate at a given pressure. This line was found by first differentiating equation 3.4 with respect to temperature, which yields:

$$\frac{dY}{dT} = \frac{\Delta H \exp\left(\frac{-E_a}{RT}\right) + E_a \exp\left(\frac{-E_a}{RT}\right)\left(\ln\frac{P}{P_o} - \frac{\Delta H}{RT} + \frac{\Delta S}{R}\right)}{RT^2} \tag{3.5}$$

Setting the right side of equation 3.5 equal to 0 and solving for T yields:

$$T_{Ymax} = \frac{E_a \Delta H}{E_a \Delta S + R\Delta H + E_a R \ln \frac{P}{P_o}} \tag{3.6}$$

A similar relationship can be found by starting with equation 3.3, which will result in a T_{Ymax} equation:

$$T_{Ymax} = \frac{E_a T_{ref} \Delta H}{E_a \Delta H + R T_{ref} \Delta H + E_a R T_{ref} \ln\left(\frac{P}{P_o f}\right)} \tag{3.7}$$

3.2.2 Tipping Point Temperature

Equations 3.6 and 3.7 provide the temperature corresponding to the fastest reaction kinetics at a given pressure. This value is termed the tipping point temperature and is the point where any further increase in temperature will begin to slow the kinetics of the metal hydride.

The effect of the tipping point temperature is very important for temperature dependence analysis. If a metal hydride is being hydrogenated and the hot spots are on the uphill side of the one of the lines shown in Figures 3.1 to 3.3, then the temperature gradients inside of the reactor grow since the hot spots inside the bed would be reacting faster than the cooler regions, absorbing more hydrogen and releasing more energy. On the other hand, if the hot spots are on the downhill side of the these lines, then the cooler regions would be reacting faster making the temperatures in the bed become more uniform. For this reason, knowing the tipping point temperatures is central to knowing how the temperature affects the reaction rate. If the reaction quickly reaches and crosses the tipping point temperature, than the hydride bed will naturally move toward thermal equilibrium. If the temperature never reaches the tipping point, then the hydride bed will be more likely to experience large temperature gradients.

If 3.6 and 3.7 are inverted, simpler relationships are obtained:

$$\frac{1}{T_{Ymax}} = \frac{\Delta S}{\Delta H} + R\left(\frac{1}{E_a} + \frac{\ln P/P_o}{\Delta H}\right) \tag{3.8}$$

$$\frac{1}{T_{Ymax}} = \frac{1}{T_{ref}} + R\left[\frac{1}{E_a} + \frac{1}{\Delta H}\ln\left(\frac{P}{P_o f}\right)\right] \tag{3.9}$$

If equation 2.2 is rearranged for $1/T$, the result is equation 3.10.

$$\frac{1}{T} = \frac{R \ln P}{\Delta H} + \frac{\Delta S}{\Delta H} \tag{3.10}$$

Comparing equation 3.10 to equation 3.8, it can be seen that the only difference between the equilibrium relationship and the T_{Ymax} relationship is the R/E_a term. This means

that the difference between the inverse temperature at Y_{max} and the inverse equilibrium temperature at the same pressure is equal to the value R/E_a. Thus the temperature corresponding to the maximum kinetics rate will always be less than that of equilibrium at a given pressure.

Plotting both equation 3.8 and 3.10 yields Figure 3.4.

This analysis shows that there is significant temperature dependence on the reaction rate of a metal hydride. It also demonstrates that a metal hydride will develop a divergent or convergent temperature gradient depending on its temperature relative to its tipping point temperature. Any hydride exposed to a constant pressure hydrogen source will approach, reach and pass the tipping point temperature as it approaches the equilibrium temperature, given the fact that kinetics are sufficient to generate heat at a rate faster than the heat loss rate.

3.3 Finite Difference Analysis

To better understand the heat transfer inside of the metal hydride bed, a finite difference analysis was performed. This allowed for a check on the validity of the LC model for a given bed dimension containing a given hydride.

3.3.1 Equation Development

To perform the finite difference analysis, the metal hydride bed was discretized into M subsections a distance Δr_{MH} apart and the container was discretized into N subsections a distance Δr_c apart. The Δr of the container and metal hydride do not need to be the same. Also, the number of spatial steps for the container can be much less than for the metal hydride since the thermal conductivity of the container will be much higher and the thickness will be much smaller. This will result in a very small temperature gradient across the container wall. Figure 3.5 shows a sample discretization.

The cylinder is assumed to have radial thermal symmetry such that there is no angular temperature dependence. The bed is also assumed to be of sufficient permeability to allow a constant pressure throughout the bed.

The one-dimensional analysis of the temperature within a cylindrical metal hydride bed with angular symmetry is described by the heat equation of the form:

$$\rho c_p \frac{\partial T}{\partial t} = \frac{1}{r}\frac{\partial}{\partial r}\left(rk\frac{\partial T}{\partial r}\right) + \dot{q} \tag{3.11}$$

where $\dot{q}$ is the energy released during the absorption of hydrogen and is defined in equation 3.12

$$\dot{q} = \frac{-\Delta H[MH]\rho_{MH}}{2MW_{MH}} \frac{dX}{dt} \tag{3.12}$$

where $[MH]$ is the number of metal atoms in one metal hydride molecule and $\frac{dX}{dt}$ is defined by equations 2.1 and 2.3.

Using a first order finite difference form of equation 3.11 and rearranging for the explicit temperature at node m for the next time step $p+1$ yields:

$$T_m^{p+1} = T_m^p + \frac{\alpha \Delta t}{r_m \Delta r^2} \left[\left(r_m - \frac{\Delta r}{2} \right) T_{m-1}^p - 2 r_m T_m^p + \left(r_m + \frac{\Delta r}{2} \right) T_{m+1}^p \right] + \frac{\Delta t \dot{q}}{\rho c_p} \tag{3.13}$$

where p is the time counter, m is the radial node counter and α is $k/\rho c_p$. The value of $\dot{q}$ is evaluated at T_m^p. The above equation is also valid for the container nodes except m should be replaced by n and $\dot{q}$ is zero for the container.

There are three boundary conditions that must be satisfied. The first is for the interior node (m=1). There are two possibilities at this node. If the node is at the center of the cylinder, the boundary condition is defined by equation 3.14. If the inside boundary node is at some intermediate point (for instance if there is a tube in the center of the bed), then the boundary condition is as defined in equation 3.15.

$$T_1^{p+1} = T_1^p + \frac{4\alpha_{MH} \Delta t}{\Delta r_{MH}^2} \left(T_2^p - T_1^p \right) + \frac{\Delta t \dot{q}}{\rho_{MH} c_{p,MH}} \tag{3.14}$$

$$T_1^{p+1} = T_1^p + \frac{\alpha_{MH} \Delta t}{r_1 \Delta r_{MH}^2} \left[\left(r_1 + \frac{\Delta r_{MH}}{2} \right) T_2^p - \left(r_1 + \frac{\Delta r_{MH}}{2} \right) T_1^p \right] + \frac{\Delta t \dot{q}}{\rho_{MH} c_{p,MH}} \tag{3.15}$$

The second boundary condition is on the very outside of the cylinder ($n = N$), where convection is occurring. This node is defined by the boundary condition given in equation 3.16.

$$T_N^{p+1} = T_N^p + \frac{2\alpha_c \Delta t}{\Delta r_c^2} \left[T_{N-1}^p - T_N^p - \frac{r_N - \frac{\Delta r_c}{2}}{r_N} \frac{h}{k_c} \Delta r_c \left(T_N^p - T_\infty \right) \right] \tag{3.16}$$

Finally, the last boundary condition that needs to be addressed is for the node at the interface between the container and the metal hydride ($m = 6$ and $n = 1$). Care is needed when evaluating this node since there are energy generation on one-half of the cell and different sized radial steps that must be taken into account. Equation 3.17 provides the explicit relationship for the temperature of the node at the time step $p+1$. Note that the counter M used in the equation could be replaced with $n = 1$ since the node is shared between the container and the metal hydride.

$$T_M^{p+1} = T_M^p + \frac{2\Delta t}{\rho_{MH} c_{p,MH} \left(r_M - \frac{\Delta r_{MH}}{4}\right) \Delta r_{MH} + \rho_c c_{p,c} \left(r_M + \frac{\Delta r_c}{4}\right) \Delta r_c} \left[k_{MH} \left(r_M - \frac{\Delta r_{MH}}{2}\right) \frac{T_{M-1}^p - T_M^p}{\Delta r_{MH}} + k_c \left(r_M + \frac{\Delta r_c}{2}\right) \frac{T_{n=2}^p - T_M^p}{\Delta r_c} + \dot{q} \left(r_M - \frac{\Delta r_{MH}}{4}\right) \frac{\Delta r_{MH}}{2} \right] \quad (3.17)$$

3.3.2 Results

The first analysis performed using the finite difference method was the experiment by Muthukumar [25] modeled by Gambini et al. [17] using the LC model. The resulting temperatures at various radial locations are shown in Figure 3.6 and the concentrations are shown in Figure 3.7.

As shown, the calculated average internal temperature matches very closely to the reported experimental data. Also of note is that the temperatures in the bed are higher than T_{Ymax}, allowing for effective hydrogenation in the cooler regions.

The temperature difference between the inside node and the outer most node in the metal hydride is at most about 8°C when $(T_1 - T_\infty)$ was near 20°C and less than 3°C when $(T_1 - T_\infty)$ was less than 11°C. In other words, the temperature difference within the hydride bed was about 25% of the temperature difference $(T_1 - T_\infty)$.

The calculated average concentration is also in good agreement with the literature data. The only divergence appears to occur at the end of the experiment.

It is interesting to note that the highest temperature is always the innermost node and is at, or equal to, the equilibrium temperature. Note that all of the temperatures in the bed are above T_{Ymax} for the entire experiment. It is also observed that the lowest concentration is also the innermost node. Since the temperatures of the entire bed are above T_{Ymax}, the cooler outer nodes have much faster rates of hydrogen absorption kinetics. This leads to a divergence in hydrogen concentration until the inner temperatures decrease sufficiently to improve the kinetics.

The next experiment modeled was the $LaNi_5$ cell developed at the University of Utah. Since this cell was developed with internal thermocouple points installed, it was possible to compare the predicted temperature values to the measured temperature values. Figure 3.8 shows the temperature values inside of the bed as predicted by the finite difference model. Figure 3.9 compares the experimental data at the three thermocouples with the predicted values at the same radial distance. Figure 3.10 shows the concentrations inside the bed as predicted by the finite difference model. As was observed in the $MmNi_{4.6}Fe_{0.4}$ simultaions,

the temperatures in these studies are above T_{Ymax} and the center temperature is at or near T_{eq} for much of the time.

It is interesting to note that in this model, the temperature distribution is diverging as time progresses as opposed to converging in the last model. This has to do with the relatively low convective heat transfer rate, which is only sufficient to remove a small amount of heat from the surface nodes. This is seen in Table 3.1 where the Biot is around 0.2 for this experiment. Additionally, when compared to Figure 3.10 it can be seen that the outer nodes, while having the lowest temperature, are also the most highly hydrogenated. It can be seen that the rate of hydrogen absorption by the outer nodes is decreasing near the end of the experiment. This seems to indicate that when the hydrogenation of the outer nodes is nearly complete, the temperatures in the bed will begin to diverge more rapidly because the heat generation at the surface nodes will cease.

Figure 3.9 compares the experimental inside temperature data with the numerical results. The "+' sign indicates the experimental data while the solid lines indicate the numerical results. As can be seen on the plot there does seem to be agreement between the numerical and experimental temperatures throughout the experiment.

The small oscillations in the experimental temperature data, readily seen in the $r = 18.5$ mm points, is an artifact of the thermocouple probe readings. By taking measurements on the bed without hydrogen present, without convective heat transfer and after being allowed to come to equilibrium over night, it was found that these oscillations in the temperature measurements continued to occur. Most likely these oscillations come from some outside magnetic field or from the data acquisition hardware itself, but are not a phenomenon occurring within the hydride.

It is worth noting that the average bed temperature as reported by the numerical model is lower than the value found experimentally. This is due to the cooler outer nodes in the numerical model that significantly reduce the average temperature at the beginning of the experiment.

Figure 3.10 shows the predicted hydrogen concentration values within the bed. Comparing Figure 3.10 with Figure 2.9 it can be seen that the average concentration in both experiments correlates very well. This indicates that while the entire bed may be at significantly different hydrogen concentration values, the average concentration of the bed can be predicted by the LC model.

In addition to the two one bed, constant pressure experiments, the magnesium hydride from the two bed experiment was analyzed. Since the pressure in the bed varied throughout the experiment, a constant pressure of 20 bar was simulated. This was chosen since it was

the maximum pressure in the bed and would also result in the largest temperature gradient. Figure 3.11 shows the temperature values inside of the bed.

It is immediately obvious that there were substantial temperature gradients within this hydride bed throughout the experiment. The average bed temperature is substantially higher than the surface temperature, with maximum temperatures in the bed exceeding 350 °C. It is also worth noting that the maximum temperature remains nearly constant at its peak during a period of about 70 seconds. This is because the conductivity is so low that heat cannot be removed from this node. The node reaches the equilibrium temperature and remains there unchanging until the adjacent temperatures drop sufficiently to allow heat transfer.

When comparing the surface temperature in Figure 3.11 with the temperature predicted by the LC model in Figure 2.11, it is clear that the temperatures increase much faster with the finite difference model. This difference is not solely due to the fact that the pressure in the finite difference model is a constant 20 bar. There is sharp rise in the surface temperature at 50 seconds in the finite difference model due to the rapid kinetics of the interior nodes. Examining Figure 2.12 the pressure in the experiment did not drop substantially from the initial 20 bar for nearly 50 seconds. This difference indicates that for the $MgH_2-0.1TiH_2$ the kinetics properties used in the LC model and in the finite difference models may be inaccurate.

Figure 3.12 shows the concentration in the bed over the length of the experiment according to the finite difference model. A very interesting feature of the figure is the plateaus observed at the innermost nodes. As stated above, when the temperature of the inner nodes reach their maximum, the temperature of the node is essentially at the equilibrium temperature. This causes the hydrogenation at the node to stop until there is sufficient cooling to lower the temperature. That is why the innermost node, as seen in black, is the first to reach the plateau and the last to leave.

These results indicate that, while temperature gradients exist, the average value of the temperature closely matches the measured average value of the experimental data for both of the one bed experiments and justifies the use of the LC model. The results from the $MgH_2-0.1TiH_2$ hydride indicate that some materials may develop substantial temperature gradients and the LC model is not an accurate simulation.

3.4 Metal Hydride Lumped Capacitance Validity Criteria

From the finite difference analysis it is clear that even for simulations that match the experimental data, there are temperature gradients across the bed. The question then is, how can that gradient be quantified to justify the use of the LC model?

To develop a criteria for the validity of the LC method the temperature gradient within the bed is assumed to be constant. Figure 3.13 shows the locations of temperature 1 and 2. To determine the profile of the temperature gradient, the heat equation is first used, shown in equation 3.11 with the transient term set to 0. This yields equation 3.18.

$$0 = \frac{1}{r}\frac{\partial}{\partial r}\left(rk\frac{\partial T}{\partial r}\right) + \dot{q} \tag{3.18}$$

where $\dot{q}$ is the volumetric heat generation rate from hydrogen absorption defined by equation 3.12. Solving for $\dot{q}$ and recognizing that k is independent of the temperature and radius yields:

$$\frac{1}{r}\frac{\partial}{\partial r}\left(r\frac{\partial T}{\partial r}\right) = \frac{-\dot{q}}{k} \tag{3.19}$$

Integrating both sides, the following relationship is developed.

$$T = \frac{-\dot{q}r^2}{4k} + C_1 \ln r + C_2 \tag{3.20}$$

Inserting the first boundary condition of $r = 0$, as shown in Figure 3.5, yields a finite temperature T, indicating that C_1 is equal to zero. Inserting the second boundary condition of $r = R_{MH}$ and recognizing that $T = T_s$, solving for C_2 and inserting that back into equation 3.20 yields:

$$T = \frac{-\dot{q}r^2}{4k} + T_s + \frac{\dot{q}R_{MH}^2}{4k} \tag{3.21}$$

Rearranging the above equation for $T - T_s$ results in equation 3.22

$$T - T_s = \frac{\dot{q}R_{MH}^2}{4k}\left[1 - \left(\frac{r}{R_{MH}}\right)^2\right] \tag{3.22}$$

To solve equation 3.22 for the temperature distribution across the entire bed, r is set to 0 and T_{Ymax} is selected for the temperature used in the heat generation term and is defined by equation 3.6. This temperature is selected to allow for the maximum temperature difference across the bed.

Knowing the temperature difference across the bed allows for the calculation of the effective temperature ratio. The ratio is defined as follows using the temperature differ-

ence between the equilibrium temperature and ambient as a representative temperature difference:

$$\theta = \frac{T_{Ymax} - T_s}{T_{eq} - T_\infty} \tag{3.23}$$

Plugging equation 3.22 into the equation 3.23, and substituting the characteristic length, $L_c = V/A_s$, for r as in the traditional LC criteria, yields the following relationship:

$$\theta = \frac{\dot{q} L_c^2 / 4k}{T_{eq} - T_\infty} \tag{3.24}$$

The only other necessary assumption is the concentration in the bed in the kinetics equation. For a conservative approach, the concentration should be in the plateau region at a point near the transition between the low concentration and the plateau regions. A value that seems to fit this criteria for the metal hydrides selected is 0.2.

With these assumption the temperature gradient can be approximated for a given hydride under a specific hydrogen pressure.

3.4.1 Results

Using the above criteria, the validity of the analysis performed in Chapter 2 can be assessed. Table 3.2 lists the values used in the analysis along with the estimated temperature difference ratio, θ.

The first observation is that the temperature difference ratio, θ, for $MmNi_{4.6}Fe_{0.4}$ is quite small indicating that the relative gradient across the hydride bed is also small. This corresponds to what was seen in the finite difference analysis. Additionally, the temperature difference for $MgH_2{-}0.1TiH_2$ is much larger than the other two hydrides.

Based on these observations, along with the finite difference analysis performed in Section 3.3, metal hydride systems with $\theta < 1$ are recommended to be analyzed with the LC model, while systems with $3 < \theta$ are not. More information is needed to determine the validity of the LC model for metal hydride systems where $1 < \theta < 3$ as the LC model and FD analysis for the $LaNi_5$ seem accurate but the possibility for large temperature gradients exists.

One additional note is that once the bed is completely hydrogenated, the relative temperature distribution calculated above is no longer valid and the bed will now behave according to a traditional LC model. This effect can be seen in Figures 3.8 and 3.10 where the temperatures appear to be beginning to diverge at the end of the experiment and the concentration of the bed is plateauing at the outermost nodes.

3.5 Conclusion

The above analysis demonstrates that there is indeed a significant temperature dependence on the hydrogenation rate of a metal hydride. The first analysis showed that the LC model developed was not valid for any of the configurations previously modeled according to the traditional relationship between the Biot number and the temperature gradient.

The volumetric heat generation analysis showed that there is a temperature dependence for the rate of hydrogenation and that there is a temperature associated with the maximum rate of hydrogen absorption for a given pressure. This temperature was termed the tipping point temperature. It was identified that metal hydrides with high ΔH values have higher tipping point temperatures and a higher difference between the tipping point temperature and the equilibrium temperature for a given pressure. This led to the conclusion that hydrides with high ΔH values have a higher potential to develop adverse temperature gradients.

The finite difference analysis predicted what the temperature gradients would be in three different metal hydrides under constant hydrogen pressure. It demonstrated that even for experiments where the LC model accurately predicted the average bed temperature, temperature gradients existed within the bed.

Finally, using a finite difference analysis for a bed in thermal equilibrium, a criteria was developed to quantify the temperature difference across the bed. This criteria provides a simple way to verify whether or not a LC model will be able to accurately predict average bed temperatures.

Table 3.1. Biot number for various hydrides in varying configurations and convective heat transfer coefficients.

Metal Hydride	Effective Conductivity (W/m-K)	Lc (m)	h (W/m^2-K)				
			2	5	10	20	1000
$MmNi_{4.6}Fe_{0.4}$	7	5.42E-03	0.00	0.00	0.01	0.02	0.77
		2.50E-03	0.00	0.00	0.00	0.01	0.36
		4.00E-03	0.00	0.00	0.01	0.01	0.57
		6.00E-03	0.00	0.00	0.01	0.02	0.86
$LaNi_5$	0.9	1.17E-02	0.03	0.06	0.13	0.26	12.96
		2.50E-03	0.01	0.01	0.03	0.06	2.78
		4.00E-03	0.01	0.02	0.04	0.09	4.44
		6.00E-03	0.01	0.03	0.07	0.13	6.67
$MgH_2-0.1TiH_2$	0.15	4.70E-03	0.06	0.16	0.31	0.63	31.30
		2.50E-03	0.03	0.08	0.17	0.33	16.67
		4.00E-03	0.05	0.13	0.27	0.53	26.67
		6.00E-03	0.08	0.20	0.40	0.80	40.00
$TiV_{0.62}Mn_{1.4}$	0.25	4.70E-03	0.04	0.09	0.19	0.38	18.78
		2.50E-03	0.02	0.05	0.10	0.20	10.00
		4.00E-03	0.03	0.08	0.16	0.32	16.00
		6.00E-03	0.05	0.12	0.24	0.48	24.00

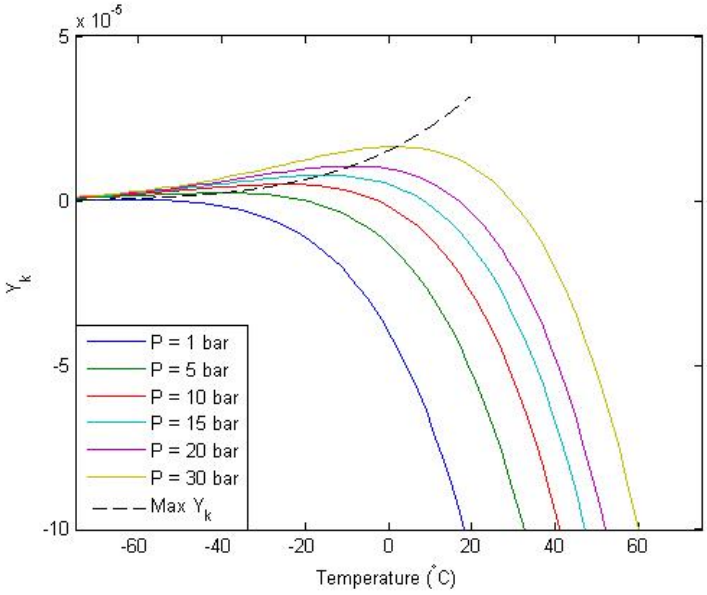

Figure 3.1. $MmNi_{4.6}Fe_{0.4}$ kinetic temperature dependence. Metal hydride reaction rate vs. temperature for $MmNi_{4.6}Fe_{0.4}$ at various hydrogen charging pressures.

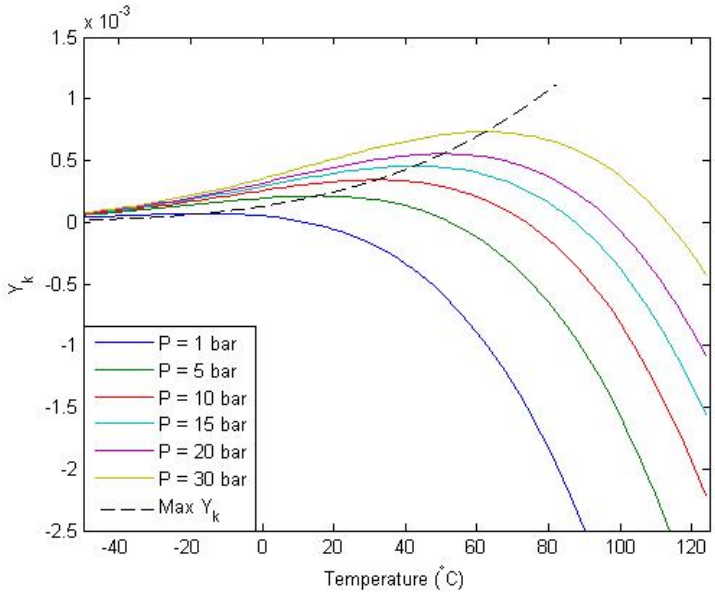

Figure 3.2. $LaNi_5$ kinetic temperature dependence. Metal hydride reaction rate vs. temperature for $LaNi_5$ at various hydrogen charging pressures.

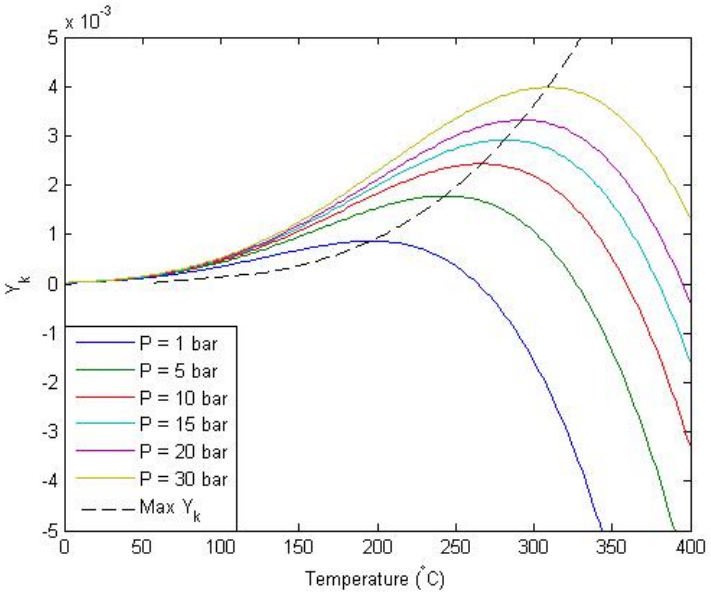

Figure 3.3. $MgH_2-0.1TiH_2$ kinetic temperature dependence. Metal hydride reaction rate vs. temperature for $MgH_2-0.1TiH_2$ at various hydrogen charging pressures.

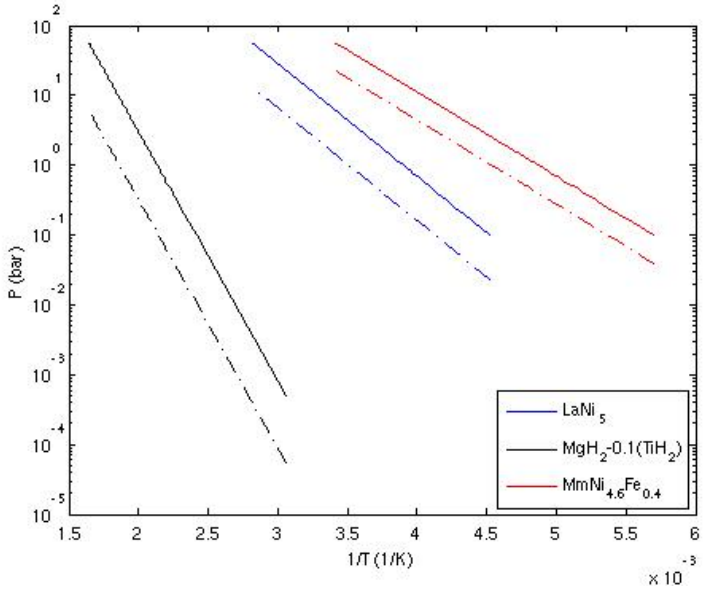

Figure 3.4. Temperature dependence of various hydrides. Van't Hoff plots showing relationship between equilibrium temperature(dotted lines) and maximum kinetics temperature (solid lines) for three different hydride alloys.

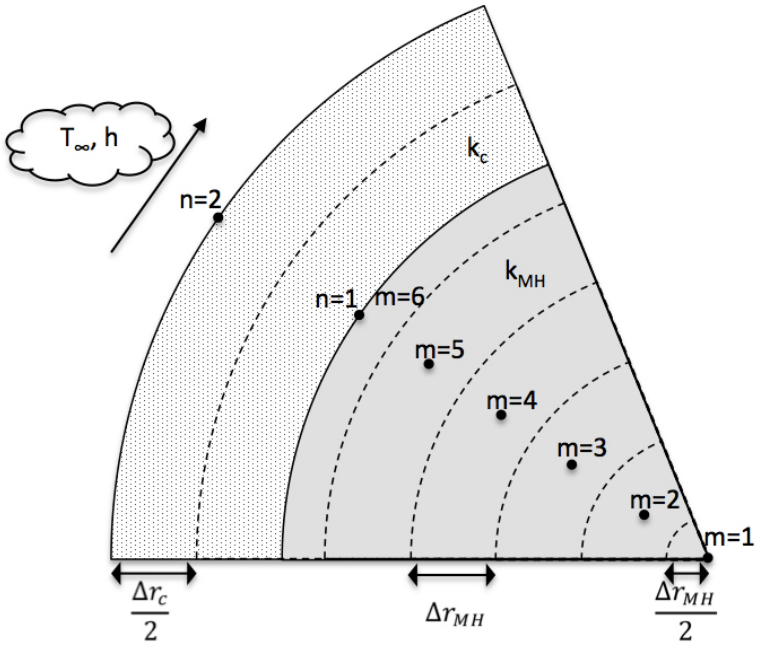

Figure 3.5. Metal hydride finite difference discretization. Sample discretization of a cylindrical metal hydride bed. In this discretization $M = 6$ and $N = 2$. The inner node is at the center of the cylinder and corresponds to the boundary condition described by equation 3.14.

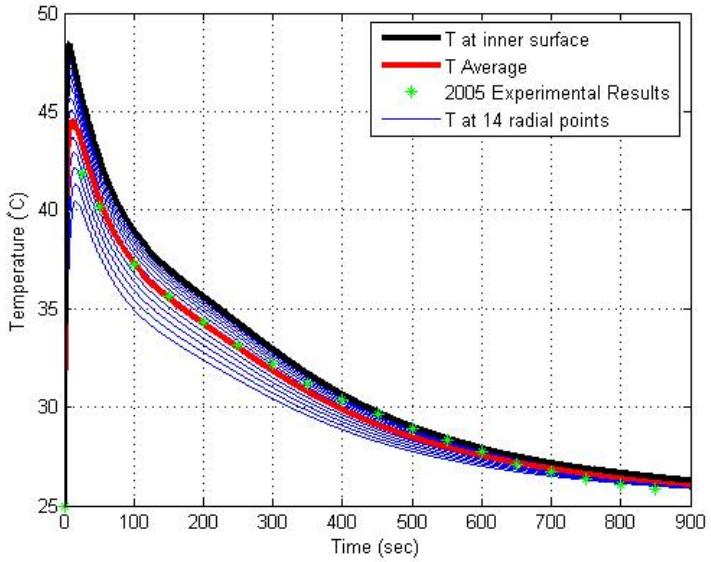

Figure 3.6. Single bed finite difference temperatures for $MmNi_{4.6}Fe_{0.4}$. Average bed temperature is compared against reported data from Muthukumar [25] for a metal hydride cell under constant pressure (P=35 bar). Analysis performed with 15 internal nodes in the metal hydride and 3 nodes in the container wall.

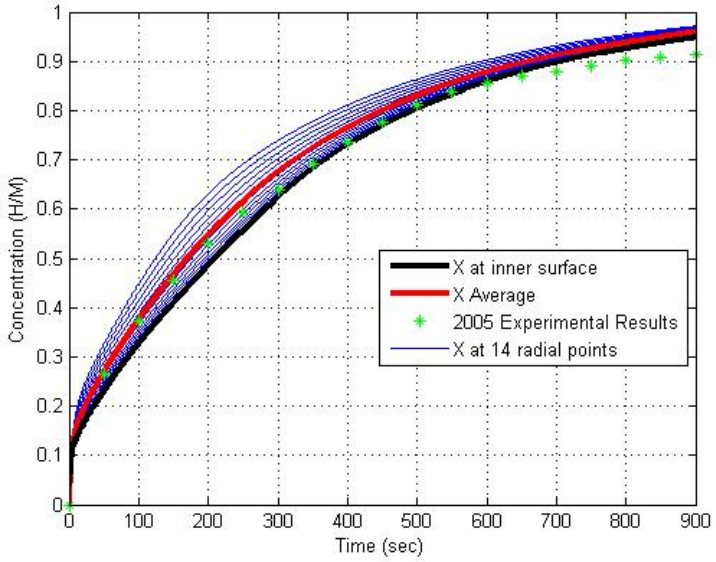

Figure 3.7. Single bed finite difference concentrations for $MmNi_{4.6}Fe_{0.4}$. Average concentration is compared against reported data from Muthukumar [25] for a metal hydride cell under constant pressure (P=35 bar). Analysis performed with 15 internal nodes in the metal hydride and 3 nodes in the container wall.

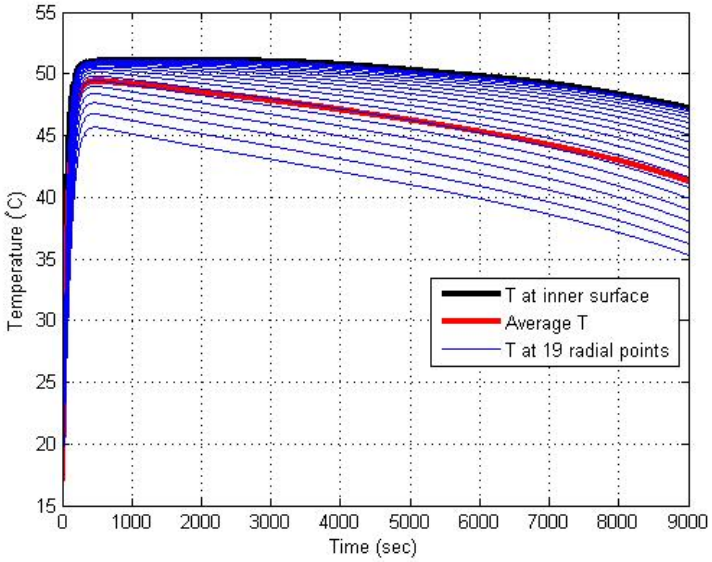

Figure 3.8. Single bed finite difference temperature for $LaNi_5$. The bed is modeled under 6 bar hydrogen pressure. Analysis performed with 20 internal nodes in the metal hydride and 5 nodes in the container wall.

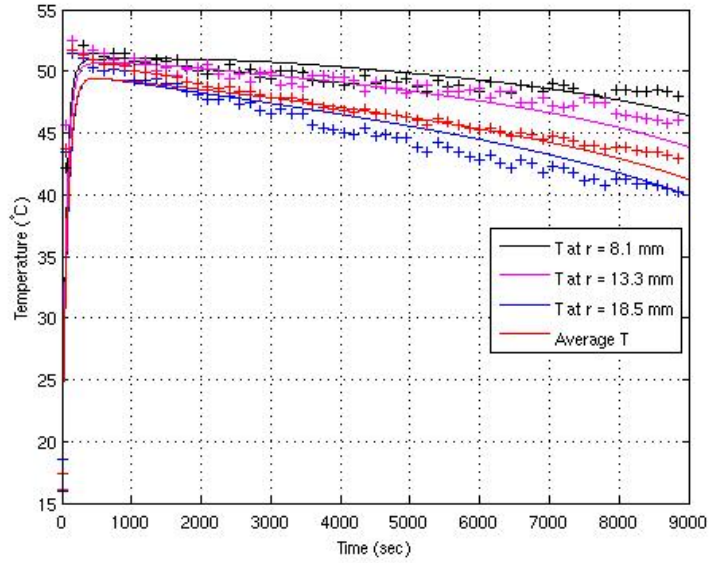

Figure 3.9. Single bed finite difference temperatures with experimental data for $LaNi_5$ temperatures. Internal bed temperatures of $LaNi_5$ at 3 internal points determined experimentally and numerically using the finite difference analysis. Experimental data are indicated by "+" symbol. The colors indicate the radial location. Analysis performed with 20 internal nodes in the metal hydride and 5 nodes in the container wall.

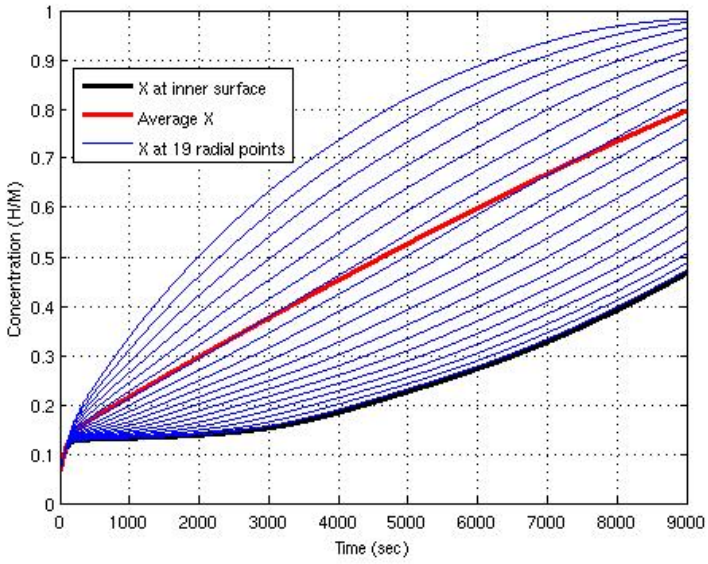

Figure 3.10. Single bed finite difference concentrations for $LaNi_5$. The bed is modeled under 6 bar hydrogen pressure. Analysis performed with 20 internal nodes in the metal hydride and 5 nodes in the container wall.

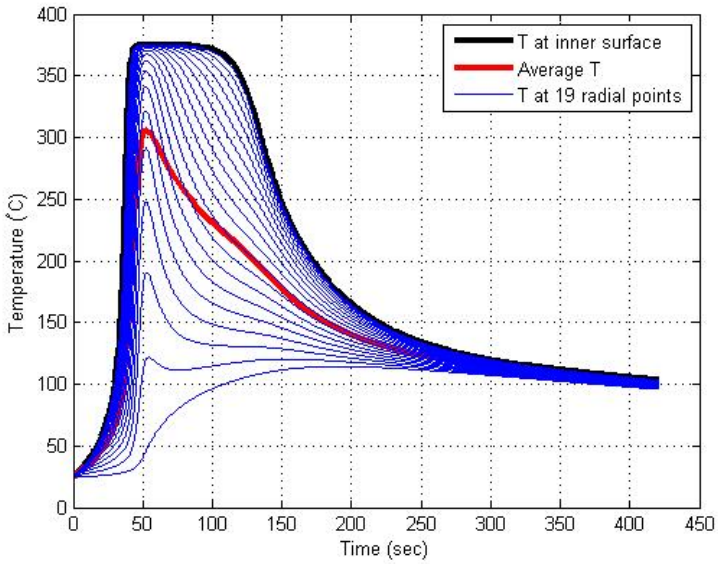

Figure 3.11. Single bed finite difference temperatures for $MgH_2{-}0.1TiH_2$. The bed is modeled under 20 bar hydrogen pressure. Analysis performed with 20 internal nodes in the metal hydride and 5 nodes in the container wall.

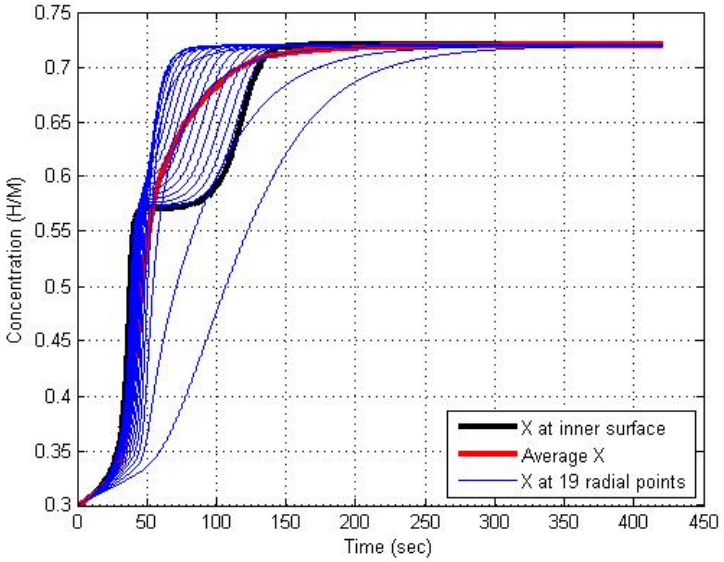

Figure 3.12. Single bed finite difference concentrations for $MgH_2-0.1TiH_2$. The bed is modeled under 20 bar hydrogen pressure. Analysis performed with 20 internal nodes in the metal hydride and 5 nodes in the container wall.

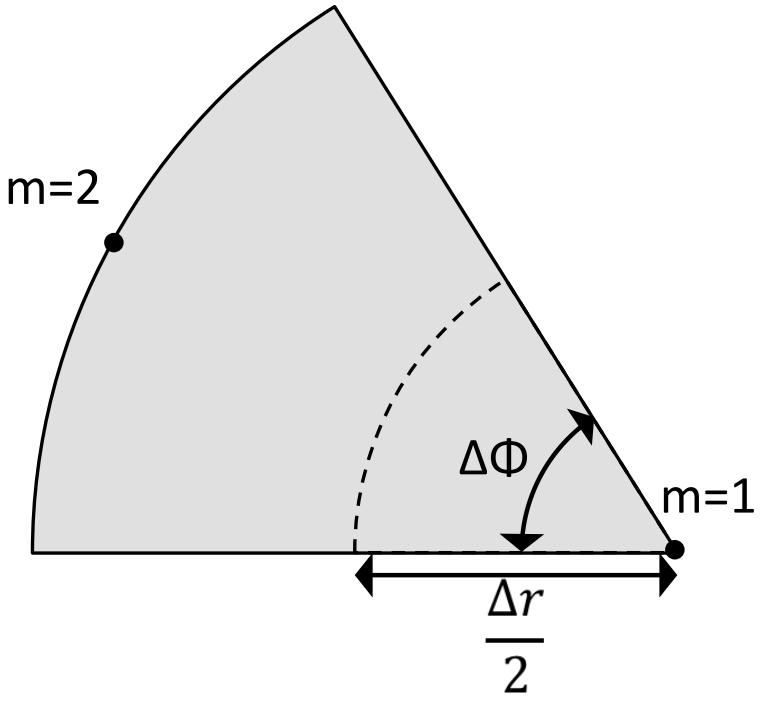

Figure 3.13. Finite difference setup on innermost node for lumped analysis cirteria

Table 3.2. Lumped capacitance validity analysis for experimental setup.

Metal Hydride	k (W/m-K)	L_c (m)	P (bar)	T_∞ (°C)	X	θ
$MmNi_{4.6}Fe_{0.4}$	5	5.42E-03	35	25	0.20	0.789
$LaNi_5$	0.9	1.17E-02	6	20	0.20	1.417
$MgH_2-0.1TiH_2$	0.15	4.70E-03	20	20	0.20	3.293

APPENDIX A

DESIGN OPTIMIZATION MATLAB CODE

```
% Metal Hydride System Design
% Gareth Whatcott
%
% Objective: To optimize the surface area, heat transfer coefficient,
% volume and metal hydride mass for each cell in a metal hydride heat pump
% array.
%
% Notes: This code uses the cold hydride as the limiting hydride based on
% the low energy density and small temperature difference on the cold bed
%

% Constants
clear;
P_out = 2.5;   % kW Required heat rate output for heating and cooling
E_out = 2.5;   % kWhr Required heat output for heating and cooling
time = 3600;       % sec Operating time

rho_cold = 8300*.4;% kg/m^3 Cold bed density
rho_hot = 1660*.69; % kg/m^3 Hot bed density
rho_ss = 8000;  % kg/m^3 Stainless steel container density
rho_ice = 916.7;% kg/m^3 Ice density

rho_air_h = 1;  % kg/m^3 Average density of air in hot bed
rho_air_c = 1.23;% kg/m^3 Average density of air in cold bed
nu_h = 20.8E-6; % m^2/s kinematic viscosity
nu_c = 13.88E-6;% m^2/s

Vol_dot = 240*4.72E-4;  % Volumetric flow rate m^3/s

e = .015E-3;    % Roughness coefficient for SS (m)

WT_cold = .0128;% Percent Cold bed weight percent
WT_hot = .065; % Percent Hot bed weight percent

cp_cold = .419; % kJ/kg-K Cold bed specific heat
cp_hot = 1.020; % kJ/kg-K Hot bed specific heat
cp_ss = .500;   % kJ/kg-K Stainless steel container specific heat
cp_air = 1.003; % kJ/kg-K Air specific heat

delH_cold = 30800;   % kJ/kmol-H2 Cold bed enthalpy of absorption
delH_hot = 68200;    % kJ/kmol-H2 Hot bed enthalpy of absorption

M_H2 = 2.0158;  % kg/kmol Molar mass of hydrogen
```

```
R = .4615;      % Gas constant for water vapor

% Variables

T_out = 35;     % C Outside air temp for cooling
T_out_cold = 15;% C OUtside air temp when heating is first needed
T_cold = 5;   % C Cold bed surface temp
T_hot = 150;    % C Hot bed surface temp
h = 20;         % W/m^2-K Heat transfer coefficient

t = .0005;       % m Thickness of fin
Po = 1.2281;    % kPa Reference water vapor pressure
To = 283;       % K Reference water vapor temperature
%max_ice = 0.01;% m Minimum spacing between fins with ice buildup
sigma_y = 170E6;% Pa Yield Strength of SS 316L
FS = 5;       % Factor of safety for hoop stress calculations
P = 20*101E3;   % Max pressure in bed
hf_o = 3/16;     % minimum fin height (inches)

L = [.3 .45 .6 .75];    % Array of lengths
N = 1:80;       % Number of cells to model



for i =1 : length(L)

    for j = 1: length(N)

% Design Equations

% Initialize optimized variables
        converge = 10;  % Convergence criterion for SS mass
        V_ss = .001;       % m^3 Volume of stainless steel container

        while converge >.1

            % Calculate mass of cold bed based on energy requirement
            m_cold =(E_out*time+V_ss*rho_ss*cp_ss*abs(T_out-T_cold))/...
                (delH_cold*WT_cold/M_H2-cp_cold*abs(T_out-T_cold));

            % Calculate mass of hot bed based on hydrogen requirement
            m_hot = m_cold*WT_cold/WT_hot;

            % Calculate required SA of cold and hot
            % beds based on heat transfer rates
            % Surface area calculations use NTU method for heat exchangers
            SA_cold = -Vol_dot*rho_air_c*cp_air*1000/h*...
                log(1-P_out/(Vol_dot*rho_air_c*cp_air*abs(T_out-T_cold)));
            SA_hot = -Vol_dot*rho_air_h*cp_air*1000/h*...
                log(1-P_out*delH_hot/delH_cold/(Vol_dot*rho_air_h*...
                cp_air*abs(T_out-T_hot)));



            % Calculate  volume of cold bed
            V_cold = m_cold/rho_cold;
            V_hot = m_hot/rho_hot;
```

```
% Loop calculates required number of fins and minimum fin
% height to achieve required surface area
SA_calc = 0;
hf_c = (hf_o-1/32)*.0254; % Fin height (m)
while SA_calc < SA_cold

    % Increment the fin height
    hf_c = hf_c+1/32*.0254;

    % Calculate the inside radius of cylinder
    ri_c = sqrt(V_cold/(pi()*L(i)*N(j)));

    % Calculate the thickness based on hoop stress
    d_c = FS*P*ri_c/(sigma_y);

    ro_c = ri_c+d_c;
    % Calculate the number of fins
    n_c = ceil((SA_cold + L(i)*N(j)*(t-2*pi*ro_c))/(L(i)*N(j)*...
        (2*hf_c-t)));
        % Make sure there is sufficient space on cell to fit
        % all the fins
        if N(j)*(ro_c+hf_c/2)^2*sqrt(12)<=pi*ro_c^2+n_c*t*hf_c
            continue;
        else
            % Calculate surface area of finned cylinder
            SA_calc = L(i)*N(j)*(2*pi*ro_c+2*n_c*hf_c-...
                (n_c+1)*t);
        end
        % This section calculates ice thickness to verify air flow
    Ql_dot = P_out/N(j);
    hfg = 2453.9+47.4*(20-T_out_cold)/20;
    hgs = hfg + 333.7;
    Psat_in = Po*exp(hfg/R*(1/To-1/(T_out_cold+273)));
    Psat_out = Po*exp(hfg/R*(1/To-1/(T_cold+273)));
    om_in = 0.622*Psat_in/(101.42-Psat_in);
    om_out = 0.622*Psat_out/(101.42-Psat_out);

    mdot_air = Ql_dot/(cp_air*abs(T_out_cold-T_cold) + (om_in - om_out)*hgs);
    m_ice = (om_in-om_out)*mdot_air*time;

    a = N(j)*rho_ice*L(i)*(pi-2*n_c);
    b = N(j)*rho_ice*L(i)*(ro_c*pi+hf_c*2*n_c-t*n_c);
    c = -m_ice;
    delta = (-b+sqrt(b^2-4*a*c))/(2*a);
    %Makes sure that there is sufficient space on the cell for
    %the fins with the ice built up
    if (2*pi*ro_c-n_c*t)/n_c <3*delta
        SA_calc = 0;
    end

end


Vss_new = N(j)*L(i)*(pi*(ro_c^2-ri_c^2)+n_c*t*hf_c);

converge = abs(Vss_new-V_ss)/Vss_new;

V_ss = Vss_new;
```

```
end

Vss_c = V_ss;

SA_calc_c = SA_calc;

% Repeat above calculations for hot bed
SA_calc = 0;
hf_h = (hf_o-1/16)*.0254; % Fin height (m)
while SA_calc < SA_hot

    % Increment the fin height
    hf_h = hf_h+1/16*.0254;

    % Calculate the inside radius of cylinder
    ri_h = sqrt(V_hot/(pi()*L(i)*N(j)));

    % Calculate the thickness based on hoop stress
    d_h = FS*P*ri_h/sigma_y;

    ro_h = ri_h+d_h;

    n_h = ceil((SA_hot + L(i)*N(j)*(t-2*pi*ro_h))/(L(i)*N(j)*...
            (2*hf_h-t)));

    if N(j)*(ro_h+hf_h/2)^2*sqrt(12)<=pi*ro_h^2+n_h*t*hf_h
        continue;
    else
         % Calculate surface area of finned cylinder
        SA_calc = L(i)*N(j)*(2*pi*ro_h+2*n_h*hf_h-...
                    (n_h+1)*t);
    end

    if (2*pi*ro_h-n_h*t)/n_h <3*delta
        SA_calc = 0;
    end

end


Vss_h = N(j)*L(i)*(pi*(ro_h^2-ri_h^2)+n_h*t*hf_h);


SA_calc_h = SA_calc;

% This sections calculates the pressure drop for the cold bed
At_c = N(j)*sqrt(12)*(ro_c+hf_c/2)^2;
Ao_c = N(j)*(pi*ro_c^2+n_c*hf_c*t);
Af_c = At_c-Ao_c;

P_c = N(j)*(2*pi*ro_c+2*n_c*hf_c);
% Hydroaulic diameter
Dh_c = 4*Af_c/P_c;
% Air velocity
V_c = Vol_dot/Af_c;
% Reynolds number
Re_c = V_c*Dh_c/nu_c;
% Friction factor
f_c = colebrook(Re_c,e);
```

```
        % Pressure drop
        DelP_c = f_c*L(i)*V_c^2*rho_air_c/(Dh_c*2);

        % Repeats above calculation for hot bed
        At_h = N(j)*sqrt(12)*(ro_h+hf_h/2)^2;
        Ao_h = N(j)*(pi*ro_h^2+n_h*hf_h*t);
        Af_h = At_h-Ao_h;

        P_h = N(j)*(2*pi*ro_h+2*n_h*hf_h);

        Dh_h = 4*Af_h/P_h;

        V_h = Vol_dot/Af_h;

        Re_h = V_h*Dh_h/nu_h;

        f_h = colebrook(Re_h,e);

        DelP_h = f_h*L(i)*V_h^2*rho_air_h/(Dh_h*2);


        % Store all values and repeat the calculation for the next length
        % or number of cells
        Tcold_output_final(j,i) = Tcold_output;
        n_cold_final(j,i) = n_c;
        n_hot_final(j,i) = n_h;
        m_hot_MH(j,i) = m_hot;
        m_cold_MH(j,i) = m_cold;
        t_h_final(j,i) = ro_h-ri_h;
        t_c_final(j,i) = ro_c-ri_c;
        ro_h_final(j,i) = ro_h;
        ro_c_final(j,i) = ro_c;
        delta_ice_final(j,i) = delta;
        PresDrop_c(j,i) = DelP_c;
        PresDrop_h(j,i) = DelP_h;
        hf_h_final(j,i) = hf_h;
        hf_c_final(j,i) = hf_c;
        thinwall_h(j,i) = 5*t_h_final(j,i)/ro_h_final(j,i);
        thinwall_c(j,i) = 5*t_c_final(j,i)/ro_c_final(j,i);

        V_cold_final(j,i) = L(i)*N(j)*sqrt(12)*((ro_c+hf_c/2)^2);
        V_hot_final(j,i) = L(i)*N(j)*sqrt(12)*((ro_h+hf_h/2)^2);
        m_cold_final(j,i) = m_cold+(Vss_c)*rho_ss;
        m_hot_final(j,i) = m_hot+(Vss_h)*rho_ss;

    end

end

% Performs cost analysis based on the cost parameters below
cost_L = .1;
cost_N = .5;
cost_n = .4;

for i = 1:length(L)
    for j = 1:length(N)
        for k = 1:length(N)
            for v = 1:length(L)
                cost(k,v) = (n_cold_final(j,i)+n_hot_final(k,v))*cost_n+...
```

```
                    (j+k)*cost_N+(L(i)+L(v))*cost_L;
            end
        end
        [cost_min1, locate] = min(cost);
        [cost_min(j,i), number] = min(cost_min1);
        L_hot_min(i,j) = L(number);
        N_hot_min(i,j) = locate(number);
    end
end

% COnvert volume from m^3 to liters
V_cold_final = V_cold_final*1000;
V_hot_final = V_hot_final*1000;


figure(1);
plot(N,V_cold_final(:,1),'r');
hold on;
plot(N,V_cold_final(:,2),'k');
plot(N,V_cold_final(:,3),'b');
plot(N,V_cold_final(:,4),'m');
hold off
legend('L=30 cm','L=45 cm','L=60 cm','L=75 cms');
xlabel('Number of Cells');
ylabel('Volume (L)');
%title('Cold Bed Volume');

figure(2);
plot(N,V_hot_final(:,1),'r');
hold on;
plot(N,V_hot_final(:,2),'k');
plot(N,V_hot_final(:,3),'b');
plot(N,V_hot_final(:,4),'m');
hold off
legend('L=30 cm','L=45 cm','L=60 cm','L=75 cms');
xlabel('Number of Cells');
ylabel('Volume (L)');
%title('Hot Bed Volume');


figure(3);
plot(N,m_cold_final(:,1),'r');
hold on;
plot(N,m_cold_final(:,2),'k');
plot(N,m_cold_final(:,3),'b');
plot(N,m_cold_final(:,4),'m');
hold off
legend('L=30 cm','L=45 cm','L=60 cm','L=75 cms');
xlabel('Number of Cells');
ylabel('Mass (kg)');
%title('Cold Bed Mass');

figure(4)
plot(N,m_hot_final(:,1),'r');
hold on;
plot(N,m_hot_final(:,2),'k');
plot(N,m_hot_final(:,3),'b');
plot(N,m_hot_final(:,4),'m');
hold off
```

```
legend('L=30 cm','L=45 cm','L=60 cm','L=75 cms');
xlabel('Number of Cells');
ylabel('Mass (kg)');
%title('Hot Bed Mass');


figure(5);
plot(N,PresDrop_c(:,1),'r');
hold on;
plot(N,PresDrop_c(:,2),'k');
plot(N,PresDrop_c(:,3),'b');
plot(N,PresDrop_c(:,4),'m');
hold off;
legend('L=30 cm','L=45 cm','L=60 cm','L=75 cms');
xlabel('Number of Cells');
ylabel('Pressure Drop (Pa)');
%title('Cold Bed PRessure Drop');

figure(6);
plot(N,PresDrop_h(:,1),'r');
hold on;
plot(N,PresDrop_h(:,2),'k');
plot(N,PresDrop_h(:,3),'b');
plot(N,PresDrop_h(:,4),'m');
hold off
legend('L=30 cm','L=45 cm','L=60 cm','L=75 cms');
xlabel('Number of Cells');
ylabel('Pressure Drop (Pa)');
%title('Hot Bed PRessure Drop');

figure(7);
w=plot(N,n_hot_final(:,1),'r');
hold on;
x=plot(N,n_hot_final(:,2),'k');
y=plot(N,n_hot_final(:,3),'b');
z=plot(N,n_hot_final(:,4),'m');
hold off;
legend('L=30 cm','L=45 cm','L=60 cm','L=75 cms');
xlabel('Number of Cells');
ylabel('Number of Fins');
%title('Hot Bed Number of Fins');

figure(8);
plot(N,n_cold_final(:,1),'r');
hold on;
plot(N,n_cold_final(:,2),'k');
plot(N,n_cold_final(:,3),'b');
plot(N,n_cold_final(:,4),'m');
hold off
legend('L=30 cm','L=45 cm','L=60 cm','L=75 cms');
xlabel('Number of Cells');
ylabel('Number of Fins');
%title('Both Bed Number of Fins');

figure(9);
plot(N,hf_h_final(:,1)*1000,'r');
hold on;
plot(N,hf_h_final(:,2)*1000,'k');
plot(N,hf_h_final(:,3)*1000,'b');
```

```
plot(N,hf_h_final(:,4)*1000,'m');
hold off;
legend('L=30 cm','L=45 cm','L=60 cm','L=75 cms');
xlabel('Number of Cells');
ylabel('Fin Height (mm)');
%title('Cold Bed Fin Height');

figure(10);
plot(N,ro_h_final(:,1)*100,'r');
hold on;
plot(N,ro_h_final(:,2)*100,'k');
plot(N,ro_h_final(:,3)*100,'b');
plot(N,ro_h_final(:,4)*100,'m');
hold off
legend('L=30 cm','L=45 cm','L=60 cm','L=75 cms');
xlabel('Number of Cells');
ylabel('r (cm)');
%title('Hot Bed Outside Radius');

figure(11);
plot(N,ro_c_final(:,1)*100,'r');
hold on;
plot(N,ro_c_final(:,2)*100,'k');
plot(N,ro_c_final(:,3)*100,'b');
plot(N,ro_c_final(:,4)*100,'m');
hold off
legend('L=30 cm','L=45 cm','L=60 cm','L=75 cms');
xlabel('Number of Cells');
ylabel('r (cm)');
%title('Cold Bed Outside Radius');

figure(12);
plot(N,cost_min(:,1),'r');
hold on;
plot(N,cost_min(:,2),'k');
plot(N,cost_min(:,3),'b');
plot(N,cost_min(:,4),'m');
hold off
legend('L=30 cm','L=45 cm','L=60 cm','L=75 cms');
xlabel('Number of LT Bed Cells');
ylabel('Cost');
```

APPENDIX B

SINGLE BED LUMPED CAPACITANCE MATLAB CODE

```
% model_v.m
% Master code to simulate metal hydride temperature and hydrogen absorption
% under a constant pressure.  This code models the experiment performed by
% Muthukumar in 2005.



clear;

constants_v;
% initial conditions
intcond = [To ;xo];
%Call ODe solver
[t, postdot] = ode45('temps_v',[.01 900], intcond);

figure(1);
plot(t,postdot(:,1)-273,'k');
axis([0 900 15 45]);
grid on;
%title('Average Bed Temperature');
xlabel('Time (sec)');
ylabel('Temperature (^\circC)');
hold on;
% Experimental data published by Muthukumar
t1 = [0 25.69444444 50  100 150 200 250 300 350 400 ...
    450 500 550 600 650 700 750 800 850];
temp1 = [25 41.87436159 40.17364658 37.27783453 35.66905005 ...
    34.29009193 33.14096016 32.17568948 31.16445352 30.33707865 ...
    29.64759959 28.91215526 28.31460674 27.71705822 27.1195097  ...
    26.70582227 26.38406537 26.06230848 25.83248212];
plot(t1,temp1,'d');
legend('Numerical Results','2005 Experimental Results');
hold off;



figure(2);
plot(t,postdot(:,2));
grid on;
title('Concentration');

for j = 1:length(postdot)
```

```
    f = polyval(k,postdot(j,2));
    % Calculate the equilibrium pressure
    Peq(j) = exp(delH/Ru*(1/postdot(j,1)-1/298))*f;
    % Calculate the weight percent from the concentration
    wtper(j)=postdot(j,2)*bx/(mmh+postdot(j,2)*ax)*100;

end

figure(3);
plot(t,Peq);
grid on;
title('P Equilibrium');

figure(4)
plot(t,wtper,'k');
grid on;
title('Weight Percent');
% Experimental data for 3 different charging pressures of P = 25, 30 and 35
% bar
time = [0   50  100 150 200 250 300 350 400 450 500 ...
    550 600 650 700 750 800 850 900];
wtperdata1 = [0 0.004211416 0.005919662 0.007205074 0.008389006 ...
    0.009369979 0.010063425 0.010909091 0.011602537 0.012245243 ...
    0.012769556 0.013175476 0.013446089 0.013699789 0.013801268 ...
    0.013987315 0.014190275 0.014291755 0.014342495]*100;
wtperdata2 = [0 0.003433404 0.004752643 0.005750529 0.006630021 ...
    0.00744186  0.007932347 0.008236786 0.008676533 0.009065539 ...
    0.009539112 0.009961945 0.010215645 0.010418605 0.010638478 ...
    0.010739958 0.010841438 0.010993658 0.011095137]*100;
wtperdata3 = [0 0.002841438 0.003839323 0.00453277  0.005209302 ...
    0.005699789 0.006376321 0.006596195 0.006849894 0.007086681 ...
    0.007221987 0.007340381 0.0074926   0.007610994 0.007729387 ...
    0.007780127 0.007813953 0.007830867 0.00784778]*100;
hold on;
plot(time,wtperdata1,'d');
plot(time,wtperdata2,'d');
plot(time,wtperdata3,'d');
hold off

% temps_v.m
% Function for use with ODE solver to calculate temperature and
% concentration of metal hydride bed.


function xdot  = temps_v(t,x)
    P =35;  % Pressure (bar)
    constants_v; % call the constants
    xdot = zeros(2,1); %initialize derivatives

    % calculate the equilibrium pressure
    f = polyval(k,x(2));
    Peq = exp(delH/Ru*(1/(x(1))-1/298))*f;

    % Calculate the rate of change of concetration
    xdot(2) = C*exp(-(Ea)/(Ru*x(1)))*abs(x(2)-limit)*log(P/Peq);
    % Calculate the rate of change of temperature
    xdot(1) = (E*cpf*mf*(Tinf-x(1))+-delH*bx*xdot(2)/Mh2)/...
        (mmh*cpmh+mss*cpss+cpc*mc);
```

```
end

% constants_v.m
% Contains all the constants necessary for modeling 1 bed experiment
% performed by Muthukumr.  The metal hydride in the experiment is
% MmNi4.6Fe0.4.
%

% Specific heats J/kg-K
cpss = 500;
cpmh = 350;
cpc = 385;
cpf = 4180;

rhof = 997; % density of cooling fluid
Vf = 3.67E-5;    %m^3/sec flow rate of cooling fluid

mmh = 0.5;      % Metal hydride mass
mc = .5;        % 0.5 kg according to Solidworks model Copper mass
mss = 1.02023;  % 1.05 kg according to Solidworks model. M. Manno states
% it should be 1.02023 kg
mf = rhof*Vf;   % Mdot of cooling fluid

As= 4.665E-2;   % surface area

Mh2 = 2.0158E-3;        %Molar mass of hydrogen
Mmh = 380E-3;              %Molar mass of metal hydride (Mm is unknown but
% summation of Ni4.6Fe0.4 yields 272.2e-3 kg/mol

delH = -23000;  %Enthalpy of absorption
% PCT curve fit coefficients accrording to Askri
k = [1.086 291.262 -2471.83 13076.3 -42253.8 ...
    85214.4 -107983 83863.7 -36592 6887.85];
k = fliplr(k);
Tinf = 298;

kmh = 7;    % thermal conductivity
% overal heat transfer coefficient
U = (1/1257+16.5E-3*log(16.5/13.5)/16.2+16.5E-3*log(13.5/6)/kmh)^(-1);
NTU = U*As/(mf*cpf);
E = 1-exp(-NTU);% Heat exchanger efficiency
limit = 1.2;    % Max hydrogen concentration
xo = .04;   % Initial hydrgoen concentration

bx = 6*mmh*Mh2/(2*Mmh); % Conversion coefficinets

C = 500;    % Pre-exponential kinetics coefficients
Ea = 25000; % Activation energy
Ru = 8.314;
To = 298;
```

APPENDIX C

TWO BED LUMPED CAPACITANCE MATLAB CODE

```
% Simulation of two hydride operation
% Author: Gareth Whatcott
%
%

clear;

%call material constants and initial conditions.
constants_v;

% define initial conditions
intcond = [xoh; Toh; moh; xoc; Toc;  moc];
options = odeset('NonNegative',[1 2 3 4 5 6],'abstol',1e-9,'reltol',1e-6);
% call and solve ode using 4th order runge kutta
[t, postdot] = ode15s('temps2_v',[.01 420], intcond,options);

% find size of output solution
[row, col] = size(postdot);

for i = 1:row
% solve for other other values(P, Peq and f) along with derivatives(xdot,
% Tdot and mdot) at each time step in output
[xdot, other] = temps2_v(t(i),postdot(i,:));
% find size of output solution
[row_o, col_o] = size(other);

    for l = 1:col_o
        % store other values for specific time step
        other_eval(i,l) = other(l);
    end

    for j = 1:col
        % store derivative values for given time step
        xdot_eval(i,j) =xdot(j);
    end
end

%plot bed temperature
figure(1);
%plot(t,postdot(:,2)-273,'k');
%plot(t,postdot(:,5)-273,'-.b');
```

```
plot(t,other_eval(:,4)-273,'r');
hold on;
plot(t,other_eval(:,8)-273,'c');
% Experimental data
time_exp = 0:15:420;
temp_c = [25.9  24.4    23.9    23.5    23.3    23  22.7    22.5    ...
    22  21.4    21.1    20.4    19.8    19.1    18.1    17  16  14.9...
    14.1    13.1    12.4    11.6    11  10.2    9.9 9.7 9   8.6 8.3];
temp_h_avg = [27.48823529   28.97493464 31.13772176 33.91346405 ....
    35.64537815 38.32368814 41.5542437  45.01418768 49.36190476 ...
    52.58193744 59.28047619 65.51968254 73.45432773 80.14827264 ...
    89.01727358 95.35364146 97.86764706 99.52009337 99.29012605 ...
    101.9787013 101.8820474 102.3463713 102.8123453 103.402903  ...
    103.6386402 104.2340005 104.2770053 105.7080214 105.6738273];
plot(time_exp,temp_h_avg,'*');
plot(time_exp,temp_c,'d');
legend('Hot Bed-Numerical','Cold Bed-Numerical'...
    ,'Hot Bed-Experimental','Cold Bed-Eperimental');
grid on;
%title('Average Bed Temperature');
xlabel('Time (sec)');
ylabel('Temperature (^\circC)');
hold off;


%plot bed concentration
figure(2);
plot(t,postdot(:,1),'k');
hold on;
plot(t,postdot(:,4),'-.b');
grid on;
title('Concentration');
xlabel('Time (sec)');
ylabel('Concentration([H]/[M])');
legend('Hot Bed - Model','Cold Bed - Model');
hold off;


for j = 1:length(postdot)

    fh = polyval(kh,postdot(j,2));
    % calculate weight percent given X
    wtperh(j)=postdot(j,1)*bxh/(mmhh+postdot(j,1)*bxh)*100;

end


figure(3);
plot(t,other_eval(:,3),'k');
hold on;
% experimental data
P_exp = [20.85  19.85   19.85   18.85   17.85   17.85   16.85   ...
    15.85   14.85   13.85   12.35   10.85   9.85    8.85    6.85...
    5.85    5.85    4.85    3.85    3.35    2.85    2.85    2.85...
    2.85    2.85    2.85    2.85    2.85    2.85];
plot(time_exp,P_exp,'h');
plot(t,other_eval(:,7),'-.b');
grid on;
%title('Bed Pressure');
```

```
xlabel('Time (sec)');
ylabel('Pressure (bar)');
legend('Bed Pressure—Numerical','Bed Pressure—Experimental');
hold off

% figure(5);
% plot(t,xdot_eval(:,1),'k');
% hold on;
% plot(t,xdot_eval(:,4),'—.b');
% grid on;
% title('Xdot');
% xlabel('Time (sec)');
% ylabel('Xdot');
% legend('Hot Bed','Cold Bed');
% hold off;
%
% figure(6);
% plot(t,postdot(:,3),'k');
% hold on;
% plot(t,postdot(:,6),'—.b');
% hold off;
% grid on;
% title('Hydrogen Mass');
% xlabel('Time (sec)');
% ylabel('mass (kg)');
% legend('Hot Bed','Cold Bed');


% figure(6)
% plot(t,wtperh,'k');
% grid on;
% title('Weight Percent');

% temps2_v.m
% Function for use with ODE solver to calculate temperature and
% concentration of metal hydride heat pump.  The flow of hydrogen between
% the beds is calculated based on the bed pressure.



function [xdot, other]  = temps2(t,x)

    % x(1) = concentration hot hydride
    % x(2) = temperature hot hydride
    % x(3) = hydrogen mass hot hydride
    % x(4) = concentration cold hydride
    % x(5) = temperature cold hydride
    % x(6) = hydrogen mass cold hydride

    xdot = zeros(6,1);  % Initialize derivative output

    constants_v;          % Call Necessary Constants

    % Calculate pressure in beds in bars
    Ph = (x(3))*Rh*x(2)/(Vh*100000);
    Pc = (x(6))*Rh*x(5)/(Vc*100000);

    % Store Pressures as a variable to retrieve later
    other(3) = Ph;
```

```
other(7) = Pc;

fh = polyval(kh,x(1));

fc = polyval(kc_de,x(4));

% Store f
other(1) = fh;
other(5) = fc;

% Calculate P equilibrium for hot bed
Peqh = exp(delHh/Ru*(1/(x(2))-1/513))*fh;
% Calculate P equilibrium for cold bed
Peqc = exp(delHc/Ru*(1/(x(5))-1/293))*fc;

% Store Peq
other(2) = Peqh;
other(6) = Peqc;
% Calculate the higher bed pressure
if Pc >=Ph
    Phi = Pc;
    Plo = Ph;
    rhohi = x(6)/Vc;
    dir = 1;    % sets mass flow direction as positive going from the
                % cold bed to the hot
else
    Phi = Ph;
    Plo = Pc;
    rhohi = x(3)/Vh;
    dir = -1;   % specifies that this flow is reversed of assumed
                % direction
end

% Perform calculationg for control valve
X =(Phi-Plo)/Phi;
if X>=xt*1.007
    mdot = 0.667*27.3*Cv*sqrt(1.007*xt*Phi*rhohi)/3600;
else
    mdot = 27.3*Cv*(1-X/(3*1.007*xt))*sqrt(X*Phi*rhohi)/3600;
end

mdot = mdot*dir;% makes sure mass flow rate has correct direction

% sets the limit of the bed to either the upper limit or zero based on
% whether it is absorping or desorbing
if Ph>=Peqh
    limith = Cmaxh;
else
    limith = 0;
end
if Pc>Peqc
    limitc = Cmaxc;
else
    limitc = 0;
end
% Calculate surface temperatures taking into account raditions
syms Tx Ty;
Tsh = solve(Uh*(Tinfh-x(2))+5.67E-8*(Tinfh^4-Tx^4)==Ush*(Tx-x(2)));
Tsc = solve(Uc*(Tinfc-x(5))+5.67E-8*(Tinfc^4-Ty^4)==Usc*(Ty-x(5)));
```

```
    other(4) = Tsh(1);
    other(8) = Tsc(1);
    % Calculate surface temperature neglecting radiation
%     Tsh = Uh/Ush*(Tinfh-x(2))+x(2);
%     Tsc = Uc/Usc*(Tinfc-x(5))+x(5);
%     other(4) = Tsh;
%     other(8) = Tsc;

    % Concentration in bed 1
    xdot(1) = Ch*exp(-(Eah)/(Ru*x(2)))*abs(x(1)-limith)*log(Ph/Peqh);
    % Temperature in bed 1
    xdot(2) = (Ash*(Uh*(Tinfh-x(2))+5.67E-8*(Tinfh^4-Tsh(1)^4))+...
        -delHh*bxh*xdot(1)/Mh2)/(mmhh*cpmhh+mssh*cpss+cpc*mch);
    % Temperature in bed 1 without radiation
    %xdot(2) =(Ash*(hh*(Tinfh-x(2)))+-delHh*bxh*xdot(1)/Mh2)/...
    %(mmhh*cpmhh+mssh*cpss+cpc*mch);

    xdot(3) = mdot-bxh*xdot(1);     % Mass flow rate

     % Concentration in bed 2
    xdot(4) = Cc*exp(-(Eac)/(Ru*x(5)))*abs(x(4)-limitc)*log(Pc/Peqc);
     % Temperature in bed 2
    xdot(5) = (Asc*(Uc*(Tinfc-x(5))+5.67E-8*(Tinfc^4-Tsc(1)^4))+...
        -delHc*bxc*xdot(4)/Mh2)/(mmhc*cpmhc+mssc*cpss+cpc*mcopc);
    % Temperature in bed 2 without raditation
    %xdot(5) = (Asc*(hc*(Tinfc-x(5)))+-delHc*bxc*xdot(4)/Mh2)/...
    %(mmhc*cpmhc+mssc*cpss+cpc*mcopc);

    xdot(6) = -mdot-bxc*xdot(4);     % Mass flow rate


end

%Metal Hydride Hot Hydride
%Material Properties
cpss = 500;     % J/kg-K stainless steel specific heat
cpmhh = 1020;    % J/kg-K Hot hydride specific heat
cpc = 385;      % J/kg-K copper specific heat

K_ss = 16.2;      % W/m-K Thermal conductivity

Mmhh = 29E-3;   % kg/mol Molar mass of metal hydride

%Geometric Properties
Ash= 2.187E-2;   % m^2 Surface Area
mmhh = .045;        % kg mass metal hydride
mch = 0;        % kg mass copper seal
mssh = .44;  % kg mass of stainles steel container
hh = 2;         % W/m^2-K
Vh = 5.466E-5;        % m^3 Empty volume in canister

r_mh = .32*.0254;   % m radius to center of MH
r_c = .38*.0254;    % m radius to inside edge of container
r_o = .5*.0254;     % m radius to outside of container

%Kinetic Properties
delHh = -68200;  % J/mol_H2 Enthalpy of absoprtion
%Peq coefficients
kh = [538.119985595842,-6375.01081892792,33434.9827937026,...
```

```
    −102228.399883362,201932.179207401,−269813.986139865,...
    248127.110049634,−156655.904728313,66481.4953781730,...
    −18143.6177954029,2942.33973107348,−249.685806497299,...
    11.1225305303127,−0.00315472936076334];
Cmaxh = .71;   % [H/M] Concentration limit
xoh = .3;       % [H/M] Initial Concentration
Toh = 299.5;       % K Initial MH temp
Ch = 115;        % 1/sec Kinetic Coefficient
Eah = 34500;     % J/mol Activation Energy − Absorption
K_h = .15;        %W/m−K Thermal Conductivity



%Metal Hydride Cold Hydride
%Material Properties
% J/kg Specific Heats
cpmhc = 500;     % J/kg−K specific heat
Mmhc = 157E−3;   %kg/mol Molar mass of metal hydride

%Geometric Properties
Asc= 2.187E−2;   % m^2 Surface Area
mmhc = .205;        % kg cold hydride mass
mcopc = 0;      % kg copper mass
mssc = .6;  % kg stainless steel mass
hc = hh;         % W/m^2−K Heat Transfer coefficient
Vc = 11.466E−5;        % m^3 Empty volume in canister

%Kinetic Properties
delHc = −28600;  % J/mol−H2 Enthalpy of adsoprtion
%PCT CHart Coefficient 13th order polynomial fit for absorption at
%20 degrees C for TiMn1.5V0.62
kc_ab = [0];
%PCT CHart Coefficient 13th order polynomial fit for desorption at
%20 degrees C for TiMn1.5V0.62
kc_de = [27563917.4918159,−164990674.018706,438259095.028252,...
    −680661591.823866,685527670.698314,−469341052.000670,...
    222651709.218780,−73211734.7442275,16415067.7656851,...
    −2421899.68732228,220938.453798788,−11288.3674690874,...
    300.886223692924,−2.85753436548481];
Cmaxc = 1.1;   % [H/M] Concentration limit
xoc = .922;       % [H/M]Initial Concentration
Toc = 298.9;       % K Initial MH temp
Cc = 30;        % 1/sec Kinetic Coefficient
Eac = 20000;     % J/mol Activation Energy − Desorption
K_c = .25;        %W/m−k Thermal conductivity



%Universal Properties
%Environment Properties

Mh2 = 2.0158E−3; % kg/mol Molar mass of hydrogen
Tinfh = 300;      % K Environment Temp
Tinfc = 300;      % K Environment Temp
Ru = 8.314;      % J/mol−K Universal Gas constant
Rh = 4124;       % J/kg−K Hydrogen Gas Constant
```

```
%Valve Properties
Cv = 100; % defined by how open the valve is.  Specificed by manf.
xt = .7; % fixed by type of valve



%Initial Conditions

%calculates initial pressure and mass of hydrogen in hot hydride bed based
%on initial concentration

bxh = 1.3*mmhh*Mh2/(2*Mmhh); %conversion coefficient


fh = polyval(kh,xoh);
Peq_oh = exp(delHh/Ru*(1/Toh-1/513))*fh;
moh = (Peq_oh*100000)*Vh/(Rh*Toh);
% Overall heat transfer coefficients from center to ambient and from center
% to surface
Uh = (1/hh+r_o*log(r_c/r_mh)/K_h + r_o*log(r_o/r_c)/K_ss)^(-1);
Ush = (r_o*log(r_c/r_mh)/K_h + r_o*log(r_o/r_c)/K_ss)^(-1);

%calculates initial pressure and mass of hydrogen in cold hydride bed based
%on initial concentration

bxc = 3.12*mmhc*Mh2/(2*Mmhc); %conversion coefficient

fc = polyval(kc_de,xoc);
Peq_oc = exp(delHc/Ru*(1/Toc-1/293))*fc;
moc = (Peq_oc*100000)*Vc/(Rh*Toc);
% Overall heat transfer coefficients from center to ambient and from center
% to surface
Uc = (1/hc+r_o*log(r_c/r_mh)/K_c + r_o*log(r_o/r_c)/K_ss)^(-1);
Usc = (r_o*log(r_c/r_mh)/K_c + r_o*log(r_o/r_c)/K_ss)^(-1);
```

APPENDIX D

FINITE DIFFERENCE MATLAB CODE

```
% Finite analysis of cylindrical cell filled metal hydride powder.  Metal
% hydride powder simulated in this experiment is LaNi5.  The finite
% difference analysis calculates the temperature and concentration in the
% metal hydride bed in the radial direction.  The container temperature
% distribution is also calculated.

clear;

% Material Properties
cpm = 419;   % J/kg-K Specific Heat
cpc = 500;
km = 0.90;    % W/m-K Thermal Conductivity
kc = 16.2;
rhom = 7330*.69;  % kg/m^3 density
rhoc = 8000;
delH = -30000;  % J/mol H2-K Enthalpy of Absorbtion
E = 27700;  % J/mol H2 Activation Energy
Tref =298;  % K Reference temperature for PCT charts
 % Polynomial coefficients
A =  [144746.024406381,-828191.210954089,2086458.76539503,...
    -3045941.19297617,2853554.80943048,-1794716.96861824,...
    770086.389702217,-224387.368673625,43277.9748057680,...
    -5228.29057985359,353.564175603414,-7.83305728011962];
MH = 6;     % Number of metal hydride atoms in a single molecule
MW = 432.45E-3;% kg/mol Molecular weight of metal hydride
alpham = km/(cpm*rhom);
alphac = kc/(cpc*rhoc);
C =45;
Xlim = 1.08;   % H/M Hydrogen capacity

% Physical Properties
h = 15; % W/m^2-K Convective heat transfer coefficient


%radius
a = .0254;  % Outside
b = .935*.0254; % inside of container
c = 5/32*.0254; % inner tube in middle of MH

At = pi*(b^2-c^2);

R = 8.314; % J/mol-K Universal gas constant
Pr = 6; % bar Constant pressure supplied to hydride
```

```
Tinf = 293;


N = 20;     % number of radial temperature points
M = 3;
delrm = (b-c)/(N-1); % radius difference
delrc = (a-b)/(M-1);
r = c:delrm:b;
for i = N+1:N+M-1
    r(i) = r(i-1)+delrc;
end


tmax = 9000;  % max time
delt = .01;  % time step
P = tmax/delt+1;

T_o = 290;  % Initial temperature
X_o = .055; % initial concentration
T = zeros(P,N+M-1);
T(1,:) = T_o;
Tmh_avg(1) = T_o;
Xmh_avg(1) = X_o;
%xdot = zeros(M,N);
X = zeros(P,N);
X(1,:) = X_o;
Tnew = zeros(1,N+M-1);

F = 1;    % Correction factor to take into account the fact that
               % there are copper fins that are not reacting

for p = 2:P

    % Calculate the temperature and concentration inner most node
    f = polyval(A,X(p-1,1));
    Peq = exp(delH/R*(1/T(p-1,1)-1/Tref))*f;
    xdot = C*exp(-E/(R*T(p-1,1)))*log(Pr/Peq)*abs(X(p-1,1)-Xlim);
    q = -delH*MH*rhom/(2*MW)*xdot*F;
    X(p,1) = xdot*delt+X(p-1,1);
      Tnew(1) = alpham*delt/(r(1)*delrm^2)*((r(1)+delrm/2)*T(p-1,2)-...
        (r(1)+delrm/2)*T(p-1,1))+delt*q/(rhom*cpm)+T(p-1,1);

    % Calculate the temperature and concentration or intermediate nodes
    for n = 2:N-1
        f = polyval(A,X(p-1,n));
        Peq = exp(delH/R*(1/T(p-1,n)-1/Tref))*f;
        xdot = C*exp(-E/(R*T(p-1,n)))*log(Pr/Peq)*abs(X(p-1,n)-Xlim);
        q = -delH*MH*rhom/(2*MW)*xdot*F;
        X(p,n) = xdot*delt+X(p-1,n);
        Tnew(n) = alpham*delt/(r(n)*delrm^2)*((r(n)+delrm/2)*T(p-1,n+1)...
            -2*r(n)*T(p-1,n)+(r(n)-delrm/2)*T(p-1,n-1))+delt*q/...
            (rhom*cpm)+T(p-1,n);
    end

    % Calculate the temperature and concentration for outer most metal
    % hydride node
    f = polyval(A,X(p-1,N));
    Peq = exp(delH/R*(1/T(p-1,N)-1/Tref))*f;
    xdot = C*exp(-E/(R*T(p-1,N)))*log(Pr/Peq)*abs(X(p-1,N)-Xlim);
```

```
    q = -delH*MH*rhom/(2*MW)*xdot*F;
    X(p,N) = xdot*delt+X(p-1,N);

    Tnew(N) = T(p-1,N)+2*delt/(rhom*cpm*(r(N)-delrm/4)*delrm+...
        rhoc*cpc*(r(N)+delrc/4)*delrc)*(km*(r(N)-delrm/2)*(T(p-1,N-1)-...
        T(p-1,N))/delrm+kc*(r(N)+delrc/2)*(T(p-1,N+1)-T(p-1,N))/delrc+...
        q*(r(N)-delrm/4)*delrm/2);

    % Calculate the temperature for container nodes
    for m = 1:M-2

        Tnew(N+m) = alphac*delt/(r(N+m)*delrc^2)*((r(N+m)+delrc/2)*...
            T(p-1,N+m+1)...
            -2*r(N+m)*T(p-1,N+m)+(r(N+m)-delrc/2)*T(p-1,N+m-1))+T(p-1,N+m);

    end

    % Calculate the temperature for the surface of the container
    Tnew(N+M-1) = 2*alphac*delt/delrc^2*(T(p-1,N+M-2)-T(p-1,N+M-1)-...
        (r(N+M-1)...
        +delrc/2)/r(N+M-1)*delrc/kc*(h*(T(p-1,N+M-1)-Tinf)+5.67E-8*...
        (T(p-1,N+M-1)^4-Tinf^3)))+T(p-1,N+M-1);


    % Calculates the average metal hydride temperature based on a weighted
    % average of area
    ATsum = Tnew(1)*pi*((r(1)+delrm/2)^2-r(1)^2);
    for x=2:N-1
        ATsum = ATsum+Tnew(x)*pi*((r(x)+delrm/2)^2-(r(x)-delrm/2)^2);
    end
    ATsum = ATsum+Tnew(N)*pi*(r(N)^2-(r(N)-delrm/2)^2);
    Tmh_avg(p) =ATsum/At;

    % Calculates the average concentration for the metal hydride
    AXsum = X(p,1)*pi*((r(1)+delrm/2)^2-r(1)^2);
    for x=2:N-1
        AXsum = AXsum+X(p,x)*pi*((r(x)+delrm/2)^2-(r(x)-delrm/2)^2);
    end
    AXsum = AXsum+X(p,N)*pi*(r(N)^2-(r(N)-delrm/2)^2);
    Xmh_avg(p) =AXsum/At;


    T(p,:) = Tnew;

end



% Plots the data

time = 0:delt:tmax;

figure(5);
w = plot(time, T(:,1)-273,'k');
hold on;
y=plot(time,Tmh_avg-273,'r');
for i = 2:N
    plot(time,T(:,i)-273);
end
```

```
% for i = N+1:N+M-1
%
%     plot(time,T(:,i)-273,'g');
% end
set(y,'LineWidth',3);
set(w,'LineWidth',3);
xlabel('Time (sec)');
ylabel('Temperature (^\circC)');
legend('T at inner surface','Average T','T at 19 radial points');
grid on;
hold off;

figure(6) ;
v = plot(time, X(:,1),'k');
hold on;
z=plot(time,Xmh_avg,'r');
for i = 2:N
    plot(time,X(:,i));
end
set(z,'LineWidth',3);
set(v,'LineWidth',3);
xlabel('Time (sec)');
ylabel('Concentration (H/M)');
legend('X at inner surface','Average X','X at 19 radial points');
grid on;
hold off;

figure(7);
% Call the LaNi5 Experimental data and plots it against the numerical data
LaNi5_exp_data
plot(time,T(:,5)-273,'k');
hold on;
plot(time,T(:,10)-273,'m');
plot(time,T(:,15)-273),'b';
plot(time,Tmh_avg-273,'r');
w = plot(time_exp, T1mid,'+k');
o = plot(time_exp, T2mid,'+m');
v = plot(time_exp, T3mid,'+b');
u = plot(time_exp, Tmidavg,'+r');
legend('T at r = 8.1 mm','T at r = 13.3 mm','T at r = 18.5 mm',...
    'Average T');
xlabel('Time (sec)');
ylabel('Temperature (^\circC)');
grid on;
hold off;

% Experimental data from LaNi5 experiment performed in the University of
% Utah sustainable energy lab. Average values are the average temperature
% in the metal hydride along the length of the probe. The mid pont values
% are the temperatures in the middle of the metal hydride on a given
% probe.


time_exp = [0   50  150 300 450 600 750 900 1050    1200    1350    ...
    1500    1650    1800    1950    2100    2250    2400    2550    ...
    2700    2850    3000    3150    3300    3450    3600    3750    ...
    3900    4050    4200    4350    4500    4650    4800    4950    ...
    5100    5250    5400    5550    5700    5850    6000    6150    ...
    6300    6450    6600    6750    6900    7050    7200    7350    ...
```

```
    7500    7650    7800    7950    8100    8250    8400    8550    ...
    8700    8850];

T1avg = [16.3   44.1 51.6   52.1    51.6    51.2    51.4    51.3...
    50.9    50.8    50.9    50.8    50.9    50.5    50.1    49.9...
    50.1    50.4    50.0    50.1    49.5    49.4    49.9    49.9...
    49.8    49.3    49.2    49.2    49.0    49.1    49.4    49.0...
    49.1    49.0    49.3    48.8    48.5    49.1    48.7    48.9...
    48.5    48.3    48.9    48.3    48.1    48.7    48.5    48.2...
    48.6    48.6    48.3    47.7    47.8    47.5    48.0    48.0...
    47.7    47.7    47.6    47.4    47.0];

T2avg = [16.7   45.7    52.6    51.7    51.7    51.7    51.3    51.0...
    51.1    50.9    50.4    50.4    50.1    50.3    50.5    50.4...
    49.9    49.7    49.9    49.5    50.0    49.9    49.3    49.2...
    49.1    49.5    49.5    49.4    49.4    49.1    48.5    49.1...
    48.7    48.7    48.3    48.7    48.6    48.1    48.3    48.0...
    48.3    48.3    47.6    48.0    47.9    47.2    47.2    47.4...
    46.9    46.7    46.6    47.1    46.7    46.6    45.9    45.7...
    45.7    45.4    45.2    45.0    45.0];

T3avg = [18.3   44.4    51.9    51.5    50.8    50.2    50.2    50.0...
    49.8    49.7    49.4    49.4    49.2    48.8    48.2    47.9...
    48.1    48.0    47.7    47.4    46.8    46.6    46.7    46.8...
    46.5    46.1    45.8    45.6    45.2    45.2    45.3    44.6...
    44.6    44.4    44.6    44.0    43.6    43.8    43.4    43.5...
    42.9    42.6    43.1    42.3    42.0    42.5    42.0    41.8...
    41.9    41.8    41.5    40.8    40.6    40.4    40.8    40.6...
    40.0    39.9    40.0    39.5    39.2];

Tcellavg = [17.5    44.5    52.0    51.6    51.2    50.8    50.7    50.5...
    50.3    50.2    49.9    49.9    49.7    49.4    49.1    48.9...
    48.9    48.8    48.6    48.4    48.1    47.9    47.9    47.9...
    47.7    47.5    47.3    47.2    46.9    46.9    46.9    46.5...
    46.5    46.3    46.4    46.1    45.8    45.8    45.6    45.6...
    45.2    45.1    45.2    44.8    44.6    44.8    44.5    44.4...
    44.3    44.2    44.0    43.6    43.5    43.2    43.4    43.2...
    42.8    42.7    42.7    42.3    42.1];

T1mid = [16.0   42.2    51.5    52.1    51.5    51.2    51.4    51.4...
    50.8    50.7    51.0    50.8    50.9    50.4    50.0    49.8...
    50.0    50.5    49.9    50.2    49.5    49.4    50.0    50.0...
    49.9    49.2    49.1    49.1    48.9    49.0    49.6    49.0...
    49.2    49.1    49.4    48.8    48.4    49.3    48.8    48.9...
    48.5    48.3    49.1    48.4    48.2    48.9    48.8    48.3...
    49.0    48.9    48.6    47.9    48.1    47.8    48.5    48.5...
    48.3    48.4    48.5    48.3    48.0];

T2mid = [16.1   45.7    52.5    51.4    51.7    51.5    50.9    50.6...
    51.1    50.8    50.0    50.3    49.7    50.1    50.3    50.5...
    49.8    49.4    49.8    49.1    49.9    49.9    48.9    49.0...
    48.8    49.6    49.6    49.5    49.5    49.3    48.4    49.1...
    48.6    48.6    48.2    48.9    48.9    48.1    48.4    48.3...
    48.5    48.6    47.8    48.3    48.3    47.4    47.4    47.9...
    47.2    47.1    47.2    47.8    47.4    47.5    46.6    46.4...
    46.3    46.1    46.0    45.8    46.0];

T3mid = [18.5   43.5    51.5    51.1    50.3    50.0    50.1    50.0...
    49.2    49.2    49.4    49.0    49.0    48.3    48.1    47.7...
```

```
    47.7    48.0    47.3    47.5    46.8    46.5    46.9    46.6...
    46.6    45.7    45.4    45.3    45.0    44.9    45.4    44.8...
    44.9    44.6    44.6    43.8    43.5    44.2    43.8    43.4...
    43.1    42.8    43.2    42.6    42.2    42.8    42.6    41.8...
    42.3    42.2    41.8    41.1    41.2    40.8    41.2    41.2...
    40.9    40.9    40.7    40.5    40.2];

Tmidavg = [17.4 43.7    51.7    51.3    50.9    50.6    50.5    ...
    50.4    50.0    49.9    49.8    49.6    49.5    49.1    49.0...
    48.8    48.6    48.8    48.4    48.4    48.1    47.9    47.9...
    47.8    47.7    47.3    47.1    47.0    46.8    46.7    46.9...
    46.6    46.6    46.4    46.3    46.0    45.7    46.1    45.9...
    45.6    45.4    45.3    45.4    45.1    44.8    45.0    44.9...
    44.5    44.7    44.6    44.4    44.0    44.0    43.7    43.8...
    43.8    43.6    43.5    43.4    43.2    43.0];
```

REFERENCES

[1] L. E. Terry, "Us patent, 4055963," November 1977.

[2] D. Gruen, M. menelsohn, and I. Sheft, "Metal hydride as chemcial heat pump," *Solar Energy*, vol. 21, no. 2, pp. 153–56, 1978.

[3] E. Willers and M. Groll, "The two-stage metal hydride heat transformer," *Int J Hydrogen Energy*, vol. 24, no. 2-3, pp. 269–76, 1999.

[4] B. S. Sekhar, S. Pailwan, and P. Muthukumar, "Studies on metal hydride based single-stage heat transformer," *Int J Hydrogen Energy*, vol. 38, no. 17, pp. 7178–87, 2013.

[5] J. Paya, M. Linder, E. Laurien, and J. Corberan, "Dynamic model and experimental results of a thermally driven metal hydride cooling system," *Int J Hydrogen Energy*, vol. 34, no. 7, pp. 3137–84, 2009.

[6] F. Yang, G. X. Wang, Z. X. Zhang, X. Meng, and V. Rudolph, "Design of the metal hydride reactors - a review on the key technical issues," *Int J Hydrogen Energy*, vol. 35, no. 8, pp. 3832–40, 2010.

[7] US Department of Energy, "Metal hydrides," http://www1.eere.energy.gov/hydrogenandfuelcells/storage/metal_hydrides.html, 12 2008.

[8] C. Song, P. Wang, and H. A. Makse, "A phase diagram for jammed matter," *Nature*, vol. 453, no. 7195, 2008.

[9] T. C. Hales, "An overview of the kepler conjecture," http://arxiv.org/abs/math/9811071v2, November 1998.

[10] Y. A. Cengel and M. A. Boles, *Thermodynamics: An Engineering Approach*, 5th ed. McGraw Hill, 2006.

[11] J. Lu, Y. J. Choi, Z. Z. Fang, H. Y. Sohn, and E. Ronnebro, "Hydrogen storage properties of nanosized $MgH_2-0.1TiH_2$ prepared by ultrahigh-energy high-pressure milling," *JACS*, vol. 131, pp. 15 843–52, 2009.

[12] US Department of Energy, "Hydrogen storage materials database," http://hydrogenmaterialssearch.govtools.us/.

[13] H.C. Chang and L.C. Want, "A simple proof of thue's theorem on circle packing," http://arxiv.org/abs/1009.4322, September 2010.

[14] Y. A. Cengel, J. M. Cimbala, and R. H. Turner, *Fundamentals of Thermal-Fluid Sciences*, 4th ed. McGraw Hill, 2012.

[15] The Engineering Toolbox, "Fan efficiency," http://www.engineeringtoolbox.com/fans-efficiency-power-consumption-d_197.html.

[16] M. Gambini, "Performances of metal hydride heat pumps operating under dynamic conditions," *Int J Hydrogen Energy*, vol. 14, no. 11, pp. 821–30, 1989.

[17] M. Gambini, M. Manno, and M. Vellini, "Numerical analysis and performance assessment of metal hydride-based hydrogen storage systems," *Int J Hydrogen Energy*, vol. 33, no. 21, pp. 6178–87, 2008.

[18] P. Muthukumar, A. Singhal, and G. Bansal, "Thermal modeling and performance analysis of industrial-scal metal hydride based hydrogen storage container," *Int J Hydrogen Energy*, vol. 37, no. 19, pp. 14 351–64, 2012.

[19] S. S. Ahmed and S. S. Murthy, "Analysis of a novel metal hydride cycle for simultaneous heat and cooling," *Renewable Energy*, vol. 29, no. 4, pp. 615–31, 2004.

[20] E. Fedorov, Y. Shanin, and L. Izhvanov, "Simulation of hydride heat pump operation," *Int J Hydrogen Energy*, vol. 24, no. 11, pp. 1027–32, 1999.

[21] M. Raju, J. P. Ortmann, and S. Kumar, "System simulation model for high-pressure metal hydride hydrogen storage systems," *Int J Hydrogen Energy*, vol. 35, no. 16, pp. 8742–54, 2010.

[22] M. Raju and S. Kumar, "System simulation modeling and heat transfer in sodium alanate based hydrogen storage systems," *Int J Hydrogen Energy*, vol. 36, no. 2, pp. 1578–91, 2011.

[23] F. Askri, M. B. Salah, A. Jemni, and S. B. Masrallah, "Heat and mass transfer studies on metal-hydrogen reactor filled with $mm_{4.6}fe_{0.4}$," *Int J Hydrogen Energy*, vol. 34, no. 16, pp. 6705–11, 2009.

[24] ANSI, *Flow equations for sizing control valves*, ANSI/ISA Standard 75.01.01-2007.

[25] P. Muthukumar, M. prakash Maiya, and S. S. Murthy, "Experiments on a metal hydride-based hydrogen storage device," *Int J Hydrogen Energy*, vol. 30, no. 15, pp. 1569–81, 2005.

[26] O. L. Akanji and A. V. Kolesnikov, "Modeling of heat and mass transfer in $LaNi_5$ matrix during hydrogen absorption-desorption cycle," *Polish Journal of Chemical Technology*, vol. 14, no. 3, pp. 71–76, October 2012.

[27] P. Muthukumar, A. Satheesh, m. Liner, R. Mertx, and M. Groll, "Studies on hydriding kinetics of some la-based metal hydride alloys," *Int J Hydrogen Energy*, vol. 34, no. 17, pp. 7253–62, February 2009.

[28] E. Hutson and G. Sandrock, "Engineering properties of metal hydrides," *Jounral of Less Common Metals*, vol. 74, pp. 435–43, 1980.

[29] F. P. Incropera and D. P. DeWitt, *Fundamentals of Heat and Mass Transfer*, 4th ed., C. Robichaud, Ed. John Wiley and Sons, 1996.